POLITECNICO DI TORINO

Master of Science Course in
Materials Engineering for Industry 4.0

Master's Degree Thesis

Design of Experiments (DoE) for multi-material 3D printing of carbon reinforced CF PEEK and laser direct structuring LDS PEEK using FFF

Supervisors
Dr Franci Pusavec
Dr Daniele Ughues
Dr Milena Salvo
Dr. Cédric Courbon

Candidate
Soukaina Tachfouti

September 2025

Table of contents

Table of figures

Table of tables

List of abbreviations used

Abbreviation	Meaning
PEEK	Polyetheretherketone
CF	Carbon Fiber
LDS	Laser Direct Structuring
AM	Additive Manufacturing
FFF	Fiber Filament Fabrication
ABS	Acrylonitrile Butadiene Styrene
PLA	Polylactic Acid
DoE	Design of Experiment
RSM	Response Surface Methodology

1 Introduction

1.1 CubeSats and Additive Manufacturing Technology

Small satellites play an important role in today's space exploration. The need in educational, scientific and commercial fields intensified the demand for compact subsystems that are lightweight, cost effective and efficient [1]. The need for multifunctional systems that can integrate structure, power, thermal regulation and electronics is rapidly growing.
As the market for small satellites continues to expand. One pathway to growth is the usage of additive manufacturing (AM), as it enables production for complex geometries with minimized assembly, increased flexibility, enhanced functionality, and resilience against thermal and electromagnetic stresses [1]. This transformative technology promotes a shift from a "design from manufacturing" to "design for need" approach, allowing for innovation and acceleration in spacecraft production [2].
Adoption of AM in aerospace is driven by stringent requirements, one of which is part consolidation and merging multi-piece and multiple materials into single printed components [3].
Polymer based AM, particularly fused filament fabrication (FFF), has wild spread use in multifunctional small satellites structures. Among these high performance thermoplastics, polyetheretherketone (PEEK) and its fiber reinforced composites are distinguished by their ability to overcome many limitations faced by raw filaments such as acrylonitrile butadiene styrene (ABS) and polylactic acid (PLA), making it a strong candidate for 3D printing satellites platforms [4].
Despite these advances, challenges remain since components operating in outer space are exposed to extreme conditions; thermal cycling and electromagnetic radiation which affects polymers and may decrease their structural and functional performance [3] [4]. Ongoing developments in space grade polymers and manufacturing approaches offer a promising path to overcome these challenges.
In summary, leveraging additive manufacturing for small satellites technologies, combined with high performing materials such as PEEK offer a promising venue for research and development. It will lead to highly efficient platforms that are well integrated, addressing both cost and performance constraints in aerospace

1.2 Project Background

Fused Filament Fabrication (FFF) is among the most prevalent additive manufacturing (AM) techniques. It enables the production of geometrically complex products using a variety of materials with high manufacturing accuracy and flexibility.
Due to gained momentum and continuously improved technology, it has become increasingly used in the aerospace industry to produce high-performance polymers parts.

This master thesis was done with Orion Additive Manufacturing GmbH. Orion is a German company founded in 2018, specializing in printing high temperature, space-grade materials such as Polyether-ether-ketone (PEEK)), Polyphenylsulfone (PPSU) and (Polyetherimide) ULTEM. Orion's unique approach lies in the development of a patented process for 3D printing that uses thermal radiation and enables the production of parts with injection molding strength. The process is capable of eliminating porosity and producing parts with a void content of less than 0.05% or a relative density of 99.95% [5].

Orion's innovative printing method is a key aspect of AM-SPACE, a joint project between multiple institutions in academia and industry. The aim is to create a novel process for producing composite parts for space applications. Objectives include the successful introduction of LDS-activated PEEK, with laser-activatable additives for metallization, into the manufacturing workflow. As LDS allows direct application of conductive paths onto the structural panels through selective metallization. Another one is printing of multi-material panels combining natural CF PEEK, and LDS PEEK while conforming to requirements. These materials must be printed under precise settings to guarantee mechanical integrity and part stability.

1.3 Scope and Objectives

The objective of this thesis is to develop an optimization approach using Design of Experiment (DoE) for multi-material printing in Fused Filament Fabrication (FFF) using carbon-reinforced PEEK as a structural base and LDS PEEK on top as functional layer.

The major challenge in this study is printing of composite panels with a thickness around ~ 1.5 mm, that are composed of two different thermoplastics (with varying properties), and are also reliable, flat and dimensionally accurate. Switching from CF PEEK to LDS PEEK adds complexity in the form of interlayer bonding, warping and thermal gradients, all of which must be reduced to the maximum to maintain part flatness integrity.

The objectives are as follows:

1. **Material Characterization**

To examine CF-PEEK and LDS PEEK printability and compatibility during FFF printing. First by establishing a reliable methodology for printing flat CF PEEK panels and then identifying the best parameters for printing LDS PEEK on its own, before exploring the integration method of the two together.

2. Process Validation
To carry out a series of baseline tests to verify the viability of multi material deposition, and ensure consistency in print result (flatness, layer adhesion).

3. Design of Experiments (DoE) setup
To design an experimental approach to determine how key 3D printing settings affect the final product's properties.

4. Experimental testing
Conduct the testing according to DOE matrix and evaluate the results of the printed parts accordingly (flatness, dimensional accuracy)

5. Optimization and analysis
Collect and analyze the data to propose optimization settings for robust production of panels, depending on the most influential process parameters.

Scope Limitations:

The scope of this thesis is to develop an adequate printing process for multi-material panels that are flat and dimensionally accurate. It does not include detailed study of long-term mechanical performance and durability.
Although, the results from this research directly support Orion's mission to produce CubeSat panels.

1.4 Thesis Structure

The current document is structured as follows:

An introduction section that provides an overview of the work's purpose, significance, and objectives. Chapter two is a literature review of AM and FFF, high temperature polymers and analyzes associated difficulties and current trends.
Chapter 3, covers the experimental procedure, including fixed parameters and methodology-guided testing.
Chapter 4 shows the results and analysis of prints.
Chapter 5 Conclusion summarizes the findings and next work to be done

2 Theoretical foundations and literature review

2.1 Additive Manufacturing

Additive manufacturing is an innovative technology for creating complicated components from 3D model data. AM manufactures parts layer by layer using filaments, powders, and even liquids, as opposed to subtractive manufacturing, such as milling, turning or drilling. Other interpellations for additive manufacturing are 3D printing, rapid prototyping, digital fabrication, and direct manufacturing technology [6].
Techniques used include stereolithography, digital light processing, selective laser sintering, electron beam melting, fusion deposition modelling, multijet/PolyJet 3D printing, and selective laser melting. Each has its own set of qualities and benefits, depending on the purpose [7].
Selecting the right AM process and material combination requires consideration for the entire AM process, including manufacturing design constraints and understanding of the strengths and limitations of each technology.

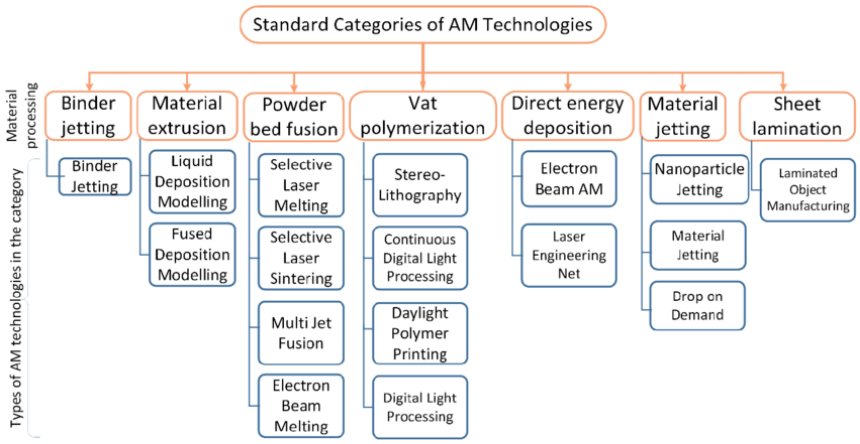

Figure 2-1: Seven categories of AM technologies

2.2 Fused Filament Fabrication

Fused Filament Fabrication (FFF) is a technology that involves the deposition of filament material as the name indicates in a sequential manner, layer by layer. The feeding mechanism drives the spooled filament through a heating element that is connected to a set of motors allowing spatial control in the build volume [8]. Once melted, the filament is forced through a nozzle by the feeder, where it is extruded at a consistent rate and cross section diameter. This Sequential deposition in FFF permits the creation of highly customizable shapes with intricate geometries while reducing the requirement for post-processing procedures [9].

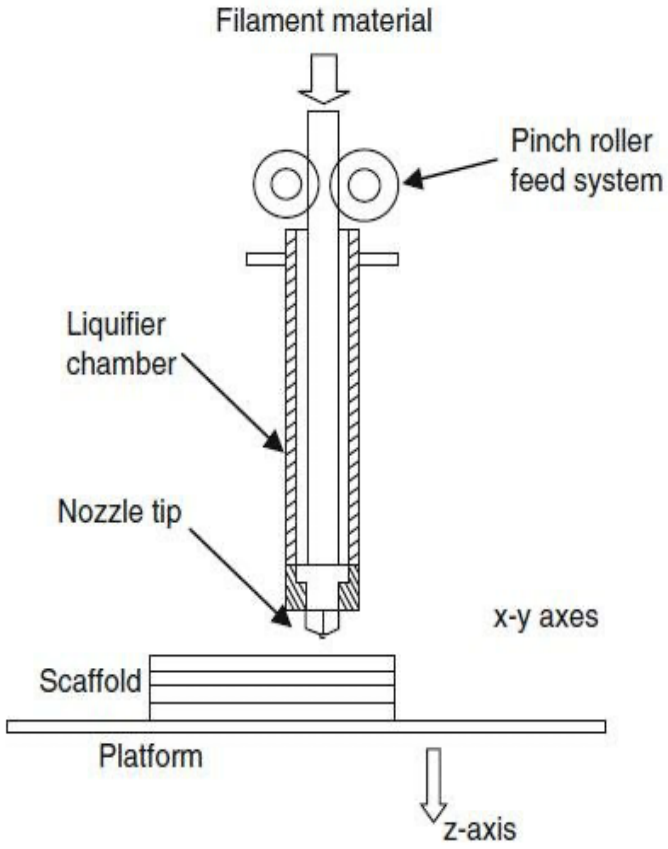

Figure 2-2: Fused Filament Fabrication

FFF can process a range of materials including thermoplastics, as well as emerging classes of composite and ceramics. Commonly used polymers include PLA, ABS, PA, PET, and TPE [10]. In addition to these, polyether ether ketone (PEEK); a high performance thermoplastic with great mechanical and chemical properties, is being used more and more in aerospace, medical and automotive fields [11] despite difficulties in processing due to high melt viscosity and extrusion temperatures [12].
Recent improvement in FFF techniques have been extended to include the use of reinforced composites and ceramic materials. One example is the development of carbon fiber reinforced PEEK (CF–PEEK) to improve stiffness and strength [12].

FFF's ability to process a wide variety of materials including different combinations offers high potential for multi-material manufacturing. These advancements leverage the production of functionally integrated parts in one build, a much-needed ability in advanced applications such as small satellites.

2.2.1 Principles of FFF

Before starting with printing, the part is first designed in CAD software such as Catia or SolidWorks, while keeping in mind the special needs and limitations of the manufacturing process. The digital models are then converted into either stereolithographic (STL) or additive manufacturing format (AMF). The next step; slicing, involves dividing the 3D model into multiple layers. Once slicing is done, a G-code is generated which controls the extruder and executes the selected settings [13].

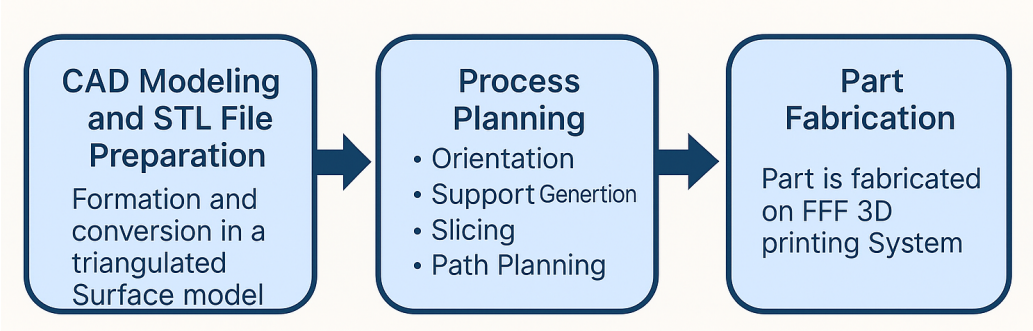

Figure 2-3: Steps of FFF printing

Printing parameters have considerable impact on part qualities like surface roughness, dimensional accuracy, and mechanical properties. FFF contains various process parameters that can be classified into three categories [14]:

Table 2-1 : Slicing Parameters of FFF

Category	**Parameter**	**Description**
Slicing Parameters	Layer height	Also known as resolution, it is the thickness of each individual extruded layer
	Raster width	Width of the deposited bead, greatly influenced by nozzle diameter
	Flow rate	Measures the amount of filament extruded every second

	Infill density	The percentage of material used to build internal components of the part
	Raster angle	The angle corresponding to the raster with regard to the bed x-axis
	Infill pattern	The pattern of the infill it can be linear, zigzag… etc.
	Air gaps	The distance between two rasters
	Contour gaps	the width of the material utilized for contours
Orientation	Build Orientation	How is the part oriented on the print bed, a bad orientation can cost surface quality and part strength
Temperature Condition	Extrusion Temperature	The temperature required to heat the filament and get it ready for extrusion
	Bed Temperature	Temperature of the build platform
	Chamber Temperature	Temperature of the chamber enclosing the print
	Layer Heater	Permits the layers to fuse together, producing stronger parts with less than 0.05% void content [5]

2.3 Thermoplastic Material – PEEK

Poly (ether-ether-ketone) (PEEK) is a melt-processable semi-crystalline engineering polymer that transitions from amorphous to crystalline structure during solidification. PEEK is one the best performing thermoplastics on the market, it exhibits outstanding structural, mechanical and thermal properties. It has the potential to replace some materials such as aluminum in certain applications due to its strong wear resistance and low friction coefficient. Furthermore, this thermoplastic is flame, smoke, and toxicity tested, making it

an advantageous material in a broad range of applications notably, aerospace, electronics, and automotive. PEEK has high resistance to thermal deterioration; its melting point is 343 °C and It can operate in environments with a temperature of up to 260 °C [15].

Table 2-2: Material properties of PEEK [16]

Item	**Value**
Density (g/cm3)	1.30
Tensile strength (MPa)	85
Shear strength (MPa)	60
Compression strength (MPa)	118
Melting temperature (°C)	343
Glass transition temperature (°C)	143
Thermal conductivity (W/ m.K)	0.25

2.3.1 Carbon Fiber reinforced PEEK

Carbon fiber reinforced PEEK (CF-PEEK) composites are becoming essential materials in aerospace applications as carbon fiber enhances PEEEK performance by improving mechanical strength, thermal resistance and dimensional stability. Carbon PEEK is highly chemically resistant and retains mechanical characteristics at temperatures up to 300ºC, making it a viable alternative to metal in some of the most extreme settings.
Overall, the addition of carbon helps in achieving a dual improvement; light weight and high strength [15].

Despite the advantageous characteristics of FDM-printed PEEK composites, the interaction of process parameters such as printing speed, layer thickness, and infill density has its own challenges and complicates the optimization of the print behavior [17]. The printing parameters have strong influence on CF-PEEK behavior results.
Additionally, the orientation of the print layers, is very important in deciding how well the print behaves, as structural anisotropy induced during printing causes different flexural and fracture performance across build orientations [18].

Generally, the usage of carbon fiber complicates the FFF printing process; the higher the filler content (%) the more brittleness and poor interlayer bonding is observed, mainly due to carbon fiber's stiffness and reduced polymer chain diffusion across layers [12]. Preheating and post processing techniques such as annealing are explored to solve these complications [19].

In conclusion, CF-PEEK offers so much potential in aerospace applications. However, maintaining consistent quality during 3D printing necessitates precise control of processing

parameters as well as mitigating of bonding difficulties. Research into optimization and hybrid fabrication processes is required for more widespread usage.

2.3.2 Laser Direct Structuring and LDS PEEK

Laser Direct Structuring (LDS) is a method that facilitates the direct transfer of electrical circuits onto part surfaces via selective laser beam etching, significantly enhancing the efficiency of development and manufacturing procedures particularly in application like CubeSat panel manufacturing which necessitates compact, lightweight and high-performance systems.

The LDS process typically go through three main steps: the fabrication of polymer part (via additive manufacturing in this case), laser ablation to activate electrical paths and then metallization [20]. First of all, the material is embedded with additives, such as organometallic compounds or mixed metal oxides, that can be activated by laser. Once irradiated with a focused laser beam, these compounds decompose, exposing catalytic metal nuclei while also roughening the polymer surface. This dual effect is essential, as it both defines the metallization pattern and facilitates adhesion for subsequent electroless plating. The laser activates the metal oxide and causes a micro rough surface that allows for a selective deposition of copper in an electroless copper bath, with optional finishes like Electroless Nickel Immersion Gold (ENIG), Electroless Nickel Electroless Palladium Immersion Gold (ENEPIG), or immersion silver achievable through standard PCB metallization techniques [21].

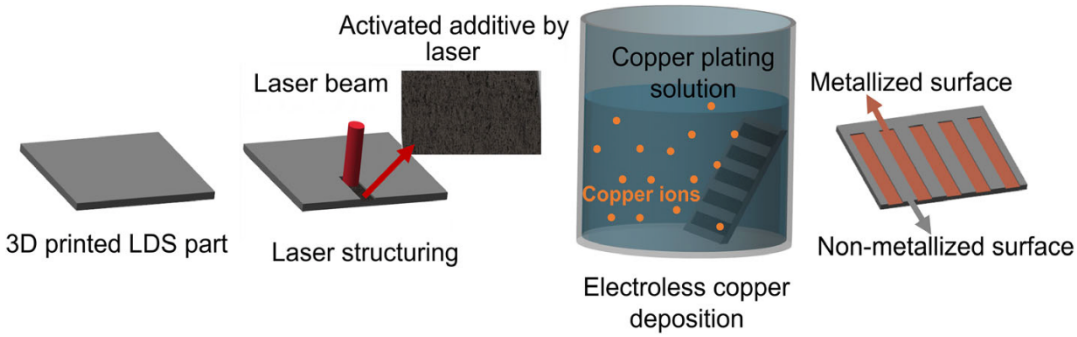

Figure 2-4: Steps of laser direct structuring (LDS)

For metallization to be effective the base material must be laser sensitive; therefore, LDS PEEK is impregnated with laser sensitive additives. This addition offers the opportunity to combine the high-performance characteristics of PEEK with a new functionality that makes it responsive to laser and allows the direct integration of electrical circuits without the need of external wiring. Therefore, it is a great way to make smart and innovative products in industries such as aerospace, where weight, size and cost are a constant struggle.

2.4 Printing Challenges

Multi-material extrusion is accompanied by a set of challenges. The most significant ones include poor bond strength between the different layers, warping issues and thermal incompatibility. And these issues become much more prominent when working with high-performance polymers like carbon-reinforced PEEK and LDS-PEEK as they directly influence dimensional accuracy, mechanical integrity, and structural reliability of printed products.

2.4.1 Warping

Warp deformation is an upward curvature that starts from the corners, consequently causing the part to shrink, contract and lift away from the plate. It is due to the residual thermal stresses, caused by the temperature variation and non-uniform cooling rate during material deposition [22]. Distortion results from the stresses caused by the continuous deposition of additional layers, especially when the adhesion between the part and build plate fails to resist the residual stresses induced pulling force [23].
A typical model expresses the relationship between shrinkage, stress and deformation:

$$\sigma_{res} = E.\alpha\,.\Delta T \tag{2.1}$$

Where:

- σ_{res} : Residual stress
- E : Young's modulus of the material
- α : Coefficient of thermal expansion
- ΔT : Thermal gradient

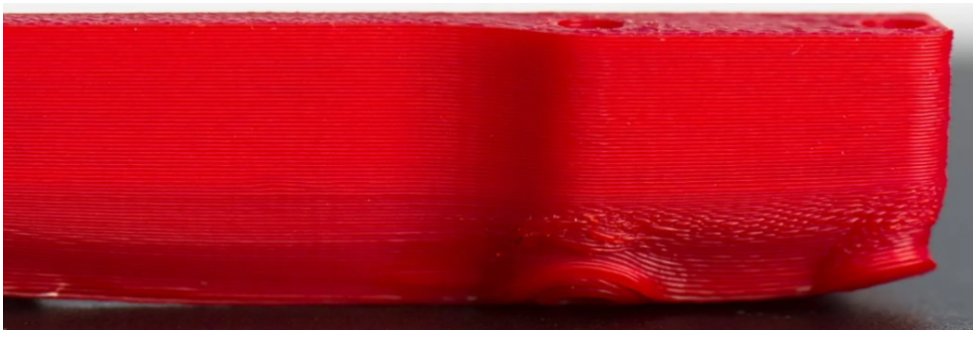

Figure 2-5: Case of warping in 3D printing

There exist four types of warping:

1. Pincushion

Solidification occurs faster on the surface than in the inner walls, resulting in the subsidence of side planes in these areas of the component [8].

2. Curling

Curling happens due to time delayed shrinking of the individual part layers resulting in various elongations and residual stresses in the part, causing an upward bending. It is usually observed at the edges of the part [8].

3. Trapezoid deformation

Surfaces of the down skin contract on their own without affecting other layers. The lower layers compress because of top layers' delayed shrinkage. Contrarily, force transfer stops subsequent layers from contracting, which leads to deformation [8].

4. Blocked shrinkage

Blocked shrinkage usually leads to geometry induced deformation. If the part has any cavities, the enclosed under-solidified material resist contractions [8].

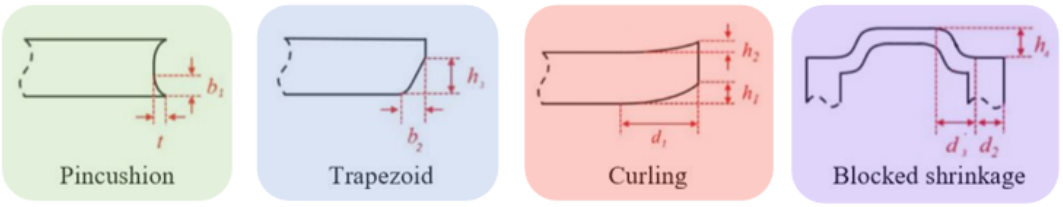

Figure 2-6: Types of warping

For a thin plate-like part, the warping force can be estimated using the following equation [24]:

$$F_w = E \,.\, \alpha \,.\, (T_1 - T_2).\, A \tag{2.2}$$

Where:

- F_w : Warping force
- E : Young's modulus of the material
- T_1, T_2 : Temperatures at the top and bottom of the part during cooling
- A : Area of the part

2.4.2 Dimensional accuracy

High-performance polymers tend to shrink significantly upon cooling, posing a challenge to achieving precise dimensional tolerances. Variables such as chamber temperature, layer height, and cooling rate all affect the final geometry of the printed part. Deviations in form

and orientation accuracy are common in complex geometries and mechanically constrained designs.
In additive manufacturing it is important to also to account for material shrinkage in the design phase to avoid parts with unwanted dimensions.

Geometrical shrinkage in FDM is usually influenced by the number of layers, section length, and material shrinkage rate. A simplified linear shrinkage model for an FDM printed layer can be expressed as [24]:

$$\varepsilon_s = \frac{L_0 - L_f}{L_0} \tag{2.3}$$

Where:

- $\boldsymbol{\varepsilon_s}$: Shrinkage strain
- L_0 : Initial length
- L_f : Final length after cooling

In semi-crystalline polymers such as PEEK, crystallization plays a dominant role in shrinkage and the associated dimensional inaccuracies. Unlike amorphous polymers, which exhibit a gradual change in volume with temperature, semi-crystalline materials undergo a sharp reduction in specific volume as molecular chains rearrange into ordered crystalline domains [25]. This crystallization-induced shrinkage is a key driver of residual stress and warpage during the additive manufacturing process. More crystallinity typically leads to greater shrinkage, and variations in crystalline morphology further influence dimensional stability. In FFF printing, differences in local crystallinity within a part are therefore the primary cause of shrinkage and warpage. To mitigate these effects, it is essential to maintain elevated processing and chamber temperatures, which slow the crystallization kinetics and promote more uniform solidification [25] [26].
Figure (2-7) represents how the volume changes progressively as temperature varies for both semi-crystalline material versus amorphous [25].

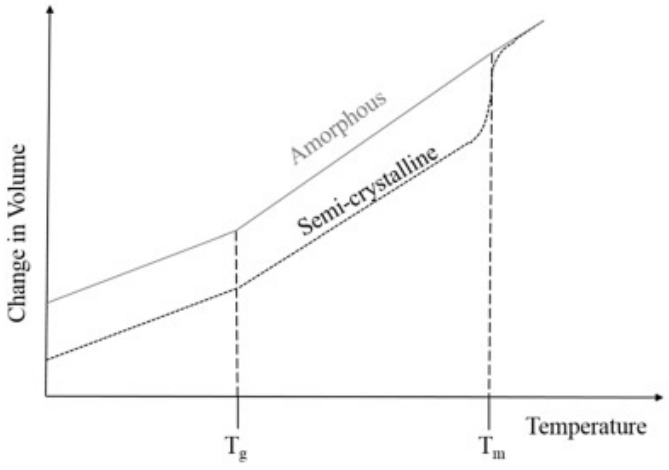

Figure 2-7: Change in volume between amorphous and semi-crystalline polymers.

2.4.3 Interlayer bonding

The quality of interlayer bonding between multiple materials depends heavily on the printing parameters (heat, print, speed, and layer thickness) and the properties of the materials themselves (thermal expansion rate, melting temperature, and whether they are chemically or thermally compatible) [27].
For example, PEEK have high melt viscosity and low surface wetting, which prevent chain diffusion and interfacial bonding with other materials. So having a dissimilarity in rheological characteristics between different materials causes incomplete fusing at the interfaces. Surface modification and localized temperature control are strategies being investigated to enhance bonding strength [28].

2.5 Design of Experiments

Design of experiments is a statistical approach that aims at establishing a link between controllable factors (input) influencing a process and the significant responses (output) resulting from them. It is an organized method for gathering and analyzing data through experiments. DoE produces a statistical correlation between the factors and responses [29].

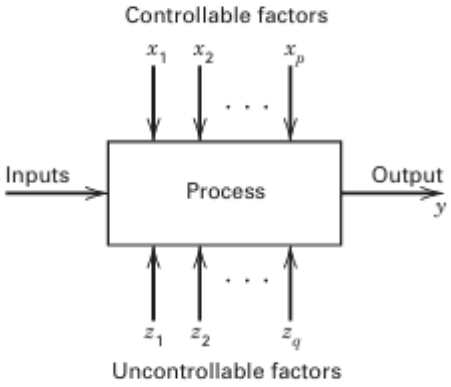

Figure 2-8: General model of a process

A traditional approach to DoE is the one factor-at-a-time (OFAT) method. The OFAT technique involves selecting a baseline set of levels for each factor and gradually altering it while keeping the other factors constant. After testing, a set of graphs are created to show how adjusting each component affects the response variable while keeping other variables constant. A significant drawback of OFAT is that it lacks consideration for potential interactions between factors.
Thus, when dealing with multiple factors, a factorial experiment is the appropriate strategy. This experimental approach involves varying multiple components simultaneously, rather than one by one [29] [30].

2.5.1 Response Surface Methodology

Response surface methodology (RSM) is a statistical method for determining and solving multivariate equations by using quantitative data from appropriate experimental designs. These equations can be represented visually as response surfaces, which can be employed in three different ways [31]:

- To describe how the test variables influence the response.
- To determine the relationships between the tests' variables.
- To describe the merged effects of all test variables on the response.

The response is well modelled using factorial approaches and ANOVA, although they are extended for more precise modelling of the effects. RSM is based on factorial research findings (screening, then three-level factorial) and is a sort of augmentation in which additional treatments are added to focus the effects and improve the model's prediction potential [31].

2.5.2 Box Behnken Method

The Box Behnken technique is an experimental design method used RSM developed in 1960. Box-Behnken designs are effective for defining experimental limits while eliminating excessive treatment combinations such as corner points and star points. BBDs designs are efficient response surface designs that provide information on experiment variables and total experimental error with minimal repetitions. They have superior symmetry and rotatability, require fewer experimental runs than traditional CCDs, and offer better insights. BBDs work with three levels (-1, 0, 1), rotatable second-order design, and can integrate numerical and categorical factors for optimization [32].

This technique is time-sensitive, affordable, and efficient, as it studies the effects of various factors using fewer experiments.

2.6 Summary and Research gaps

A review of current literature shows that a great deal of work has been done on additively manufactured high temperature thermoplastics, particularly PEEK and carbon reinforced PEEK. Existing studies have explored mechanical performance, tribological properties and crystallinity of PEEK prints under various processing conditions. Others have focused on printing parameters optimization such as extrusion temperature, chamber, speed … etc. to reduce warping and improve part stability. However, most of these studies are limited to single material parts, with little research addressing dual-material setups, particularly laser direct structured PEEK.

While LDS PEEK is widely utilized in laser-activated applications in its injection molded

form, its behavior during fused filament fabrication (FFF) is mostly unexplored, especially when printed on CF PEEK substrates. There is a significant research gap in understanding how these two materials interact, and what are the parameters and deposition conditions that influence dimensional stability and print quality in such a dual-material system. Very few studies have investigated how the temperature mismatch between CF PEEK and LDS PEEK affects warpage or how to optimize multi-material process settings to create functioning, flat parts.

This thesis seeks to fill these gaps by providing experimental insight into the combined printing of CF PEEK and LDS PEEK, resulting in a better knowledge of their compatibility and laying the framework for future research in metallizable, structurally connected components.

3 Research methodology

3.1 Overview of methodology

The experimental workflow will be divided into two phases. It will take a structured approach to allow isolation of each material's specific properties and printing needs, and to account for the additive nature of printing multiple materials in fused filament fabrication process.
The goal is to optimize the process parameters of each material by itself and define the critical inputs before the combination.

- **STEP 1: CF PEEK printing**

The focus of this first step was exclusively printing CF-PEEK panels and determining the ideal process variables, and the most influencing parameters, to produce flat and dimensionally accurate parts. Prioritizing flatness and studying the warping behavior is necessary at this step, since CF PEEK is the base material and any issues arising would directly impact the integrity of the final product.

Samples with several parameters combinations are printed using design of experiments (DoE) method to narrow down the optimal printing settings that minimize warping and surface distortion of the panels. Each print is evaluated based on flatness, dimensional accuracy in z-direction, and visual quality (uniformity and finish of the part). The resulted process window that reliably generates defect free base layers of CF PEEK will serve as foundation for the following stage.

- **STEP 2: Composite layer of LDS PEEK**

After the identification of stable CF PEEK printing conditions, this following step has for objective the deposition of LDS PEEK on the base layer and evaluating the compatibility of

these two materials when printed together and how adhesion and the overall flatness of the part are affected.

LDS PEEK deposition is systematically studied through a DoE approach as well, to understand the respective influence of each factor. Each part is evaluated based on the curling and warping that may be introduced by the second material, total panel thickness and if it falls within the targeted specification.

This methodology of initially optimizing the base material alone and subsequently adding the secondary material, meticulous facilities and controlled experiments devoid of the noise of confounding variables. It enhances the reliability of collected data, so facilitating a better understanding on how different materials interact together in high-temperature additive manufacturing processes.

3.2 Materials used

3.2.1 CF PEEK 10

CF PEEK is a premium high-performance thermoplastic composite. The 10% chopped carbon fiber reinforcement increases PEEK's stiffness, compressive strength, and load capacity. In this study, KetaSpire 10% CF PEEK AM from Solvay was used.

Table 3-1: Properties of KetaSpire 10% CF PEEK [33]

Properties	KetaSpire 10% CF PEEK AM
Diameter (mm)	1.75
Tensile Modulus (GPa)	11
Tensile Strength at break (MPa)	140
Tensile Elongation at break (MPa)	1.7
Glass Transition Temperature (C)	150
Melt Temperature (C)	340
Build Plate Temperature (C)	> 200

3.2.2 LDS PEEK

LDS PEEK is sourced from manufacturer Ensinger with the following properties:

Table 3-2: Properties of TECAFIL PEEK LDS [34]

Properties	TECAFIL PEEK LDS black
Diameter (mm)	1.75 +/- 0.05 mm
Tensile Modulus (GPa)	9.6
Tensile Strength at break (MPa)	81.3
Tensile Elongation at break (MPa)	1.7
Glass Transition Temperature (°C)	143
Melt Temperature (°C)	343
Build Plate Temperature (°C)	160 - 250

3.2.3 Storage and drying protocol

It is very important for the filament to be stored correctly. Inadequate storing environments can lead to moisture absorption, thus affecting print quality and causing a decrease in mechanical properties.
The drying recommendations are around 150 °C for about 2-4 hours. The filament rolls should be stored in dry and dark areas as they can be easily affected by the humidity in the atmosphere.

3.3 Equipment and Hardware

3.3.1 FFF machine

The Fused Filament Fabrication printer consists of an extruder with a gear system that is responsible for pulling the filament and pushing it into the hot end for melting at the appropriate temperature. The molten filament is then extruded into through a nozzle (final component of print head) onto the build platform with the required pattern and shape.
The Build Platform in this case is heated but it can be kept cool depending on the purpose. Finally, the print is surrounded by enclosing chamber, which is responsible for controlling the temperature during and after printing.

In this thesis research, we will be using Orion Additive Manufacturing A150 Series printer, with its thermal radiation heating technology, it involves using thermal radiation in all directions to efficiently heat the printed object up to 300 C [5].

Figure 3-1: Orion A150 AM printer

Table 3-3: Technical specifications of Orion A150-15 printer [5].

Build volume	180mm diameter x 150mm high
Layer Height	20µm - 400µm
Print Speed	10 mm/s - 400 mm/s
Technology	FFF - Thermal Radiation Fusion
Max extruder Temperature	500 °C
Max Bed Temperature	300 °C
Max layer heater Temperature	400 °C
Filament Diameter	1.75 mm

Materials	PEEK, PEAK, PEKK, PEI, ULTEM1010, ULTEM9085, ABS, PC, PA6, PA12, PPSF/PPSU
Motion Kinematics	Delta 3-Axis platform
Voltage	380 – 440V AC
Weight	50 Kg

3.3.2 Nozzle and Build plate specification

Nozzle type used was E3D hardened steel nozzles with diameters of 0.5 mm and 0.6 mm depending on the target layer height. According to commonly used guidelines, layer height should be between 25% - 80% of nozzle diameter.
Hardened steel nozzles were necessary due to the abrasive nature of CF-PEEK, which causes rapid wear on brass nozzles during prolonged printing.

The build plate was made out of aluminum, offering uniform thermal conductivity to support first-layer adhesion. No coating was applied.

3.3.3 Measurement Tools

3.3.3.1 Infrared Camera

An infrared (IR) thermal camera was used to monitor the temperature distribution across the print surface during and after the printing process. This tool was essential for validating the cooling strategy and identifying thermal gradients between layers, which often contribute to residual stress and warping.

3.3.3.2 Flatness Probe

Warping was assessed using flatness deviation as the primary response variable. Flatness deviation was defined as the maximum vertical displacement of any corner or edge of the printed panel from the nominal flat surface of a plate after cooling to ambient temperature.
Each printed panel was measured using dial gauge following a 9-point grid, as shown in Figure 4-3, the grid includes points labelled A through I, distributed symmetrically across the panel surface. This configuration allowed for detection of both localized and global deformation across the part surface.

Measurement Procedure

- All measurements were taken after the part had cooled to room temperature (25 ± 1°C) to ensure consistent thermal contraction across trials.
- Each point was gently probed at its center using a custom fixture to ensure contact accuracy and avoid deformation during measurement.

- The panel was placed on a certified flat granite reference plate during measurements to eliminate surface-level irregularities in the measurement environment.

The nine z-height values for each sample were used to calculate the standard deviation (σ) according to:

$$\sigma\ (mm) = \sqrt{\frac{1}{n}\sum_{i=1}^{n}(z_i - z)^2} \tag{3.1}$$

Where:

- z_i = measured height at point i
- z = average height across all nine points
- n = 9

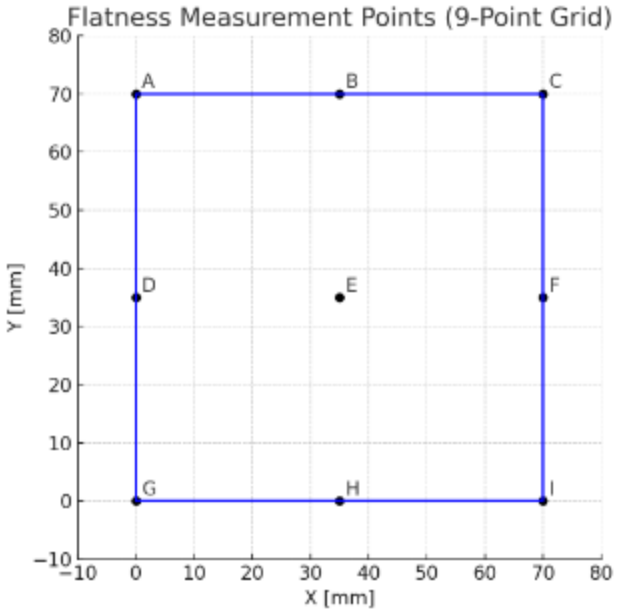

Figure 3-2: Measurement points across the panel

3.3.3.3 Dimensional Measurement

This study specifically focused on vertical dimensional accuracy as no significant trends or variations were seen in the horizontal direction (lengths of the panels sides). In the building direction (z-axis) FFF has greater residual stress and heat shrinkage than in the x-y plane. For thin components as the panel examined here, even small deviations are critical, making this important to explore exploring and the primary focus of this study.

By using vernier caliper, the thickness of each sample is measured at 3 different locations and averaged, the deviation from the target is then calculated:

$$\Delta Z\ (mm) = Z_e - Z_c \tag{3.2}$$

Where:

- Z_c= CAD dimension
- Z_e= Average experimental dimension

The percentage dimensional error is given by:

$$\Delta Z\ (\%) = \left|\frac{Z_c - Z_e}{Z_c}\right| \times 100 \tag{3.3}$$

3.4 Experimental Procedure

Sample Geometry: Before printing the full-scale CubeSat panel (1U format 100x100mm Figure 4-1), a reduced-size geometry of 70 × 70 mm was selected for the initial testing phase while keeping similar thickness (Figure 3-4).

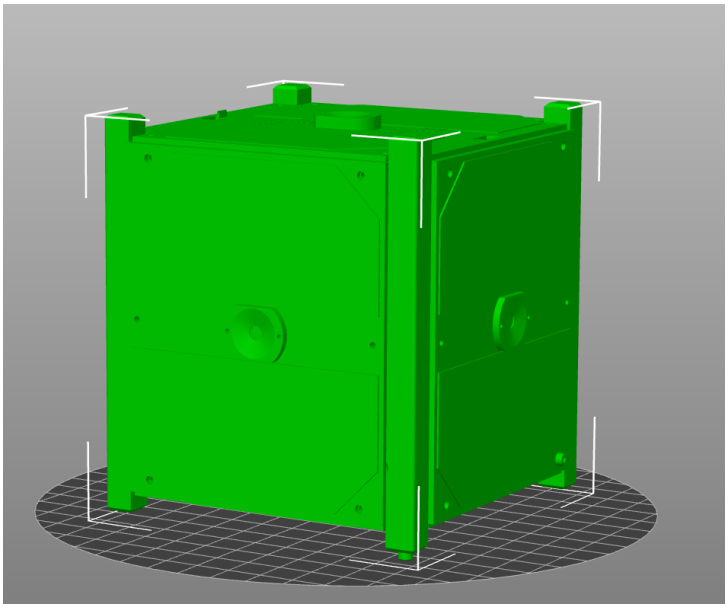

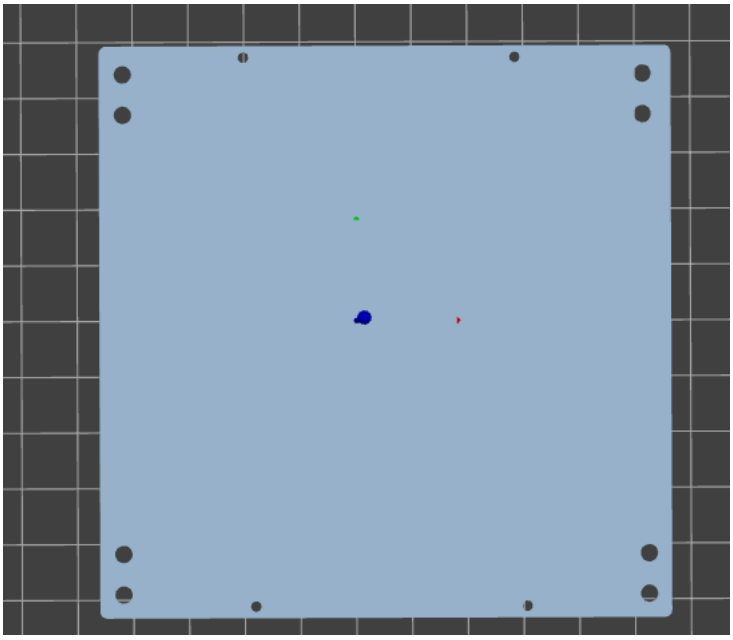

Figure 3-3: 1U CubeSat

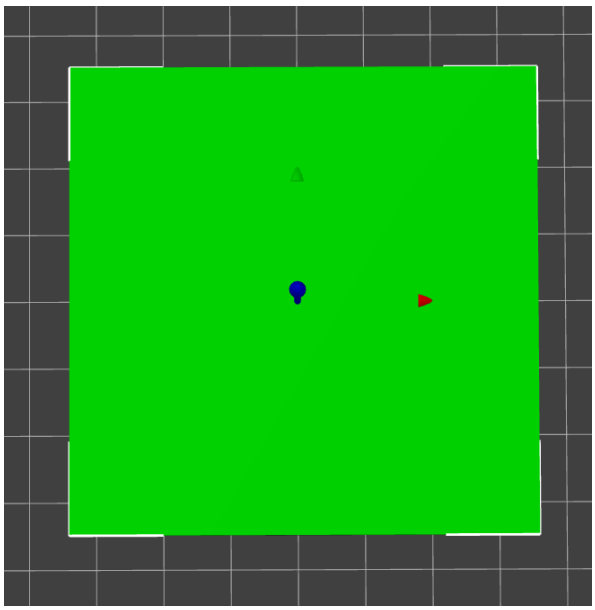

Figure 3-4: Test specimen 70 × 70 mm

The thickness of the panel should be targeted to be around 1 mm, and not exceeding 1,40 mm. For LDS PEEK to be eligible for laser activation; its thickness should be above > 0,1 mm.

3.4.1 Phase 1 – CF PEEK baseline testing

This phase focused on identifying stable process parameters for printing flat and dimensionally accurate CF-PEEK parts.

3.4.1.1 Initial parameter setting

Preliminary testing based on manufacturer recommendation, literature review aimed to identify a process window for printing CF-PEEK panels. The goal was to guide parameter selection for future DoE trials and reduce trial-and-error in dual-material printing and define at which settings CF PEEK printed properly. The starting conditions were set as follows.

Table 3-4: CF-PEEK printing parameters

Parameter	**Value**
Extruder temperature (°C)	435
Bed temperature (°C)	265
Chamber temperature (°C)	300
Layer heater (°C)	300
Nozzle diameter (mm)	0.6
Print speed (mm/s)	40
Infill density (%)	100
Layer height (mm)	0.175
Flow rate (%)	96

Flow rate was set to 96% throughout all experimental trials. The decision was made by initial extrusion calibration tests, where over-extrusion was observed at default 100% flow rate. Filaments with carbon fiber usually require slightly lower flow rates to ensure controlled melting behavior, as they are more viscous and abrasive.

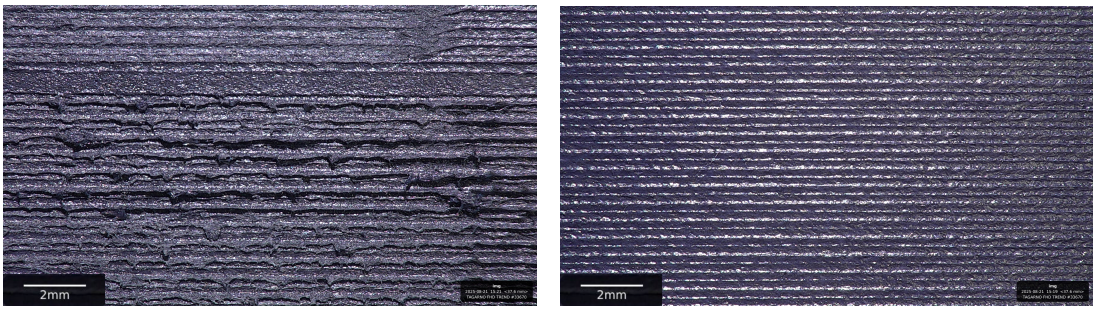

Figure 3-5: Surface quality with 100% flow rate (left), Surface quality with 96% flow rate (right)

Under these printing parameters, initial trials showed a variation of warping behaviors which highlighted the need for parameter evaluation and optimization.

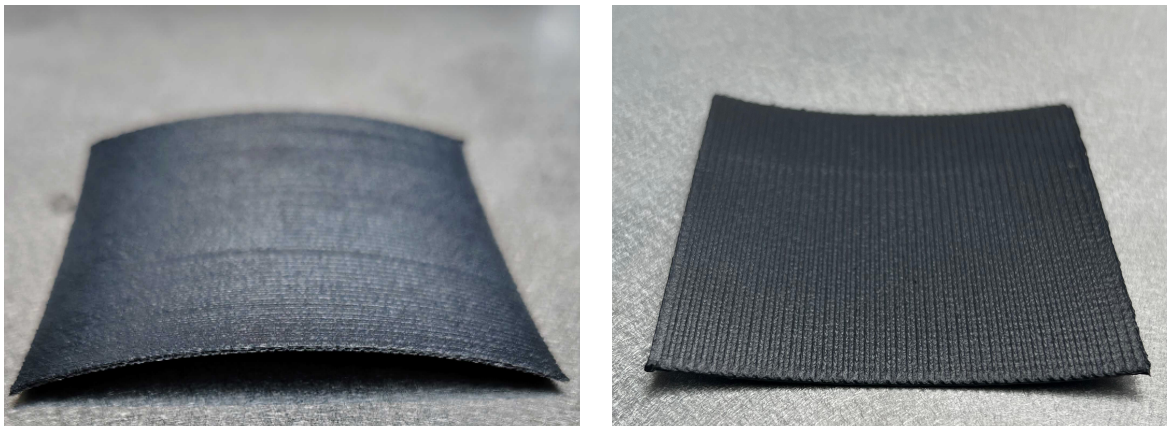

Figure 3-6: CF PEEK prints with warping behavior

3.4.1.2 Infill pattern evaluation

Additive manufacturing of semi-crystalline polymers PEEK is highly sensitive to both thermal history and the geometry of the internal structure. The way the material is deposited; its infill pattern affects how heat flows during printing and influences the directional stiffness of the final part. Multiple infill patterns were tested to determine the best baseline configuration. Prior work shows that raster orientation and infill pattern influence both stiffness anisotropy and dimensional accuracy, hence can affect distortion. The patterns compared are the following.

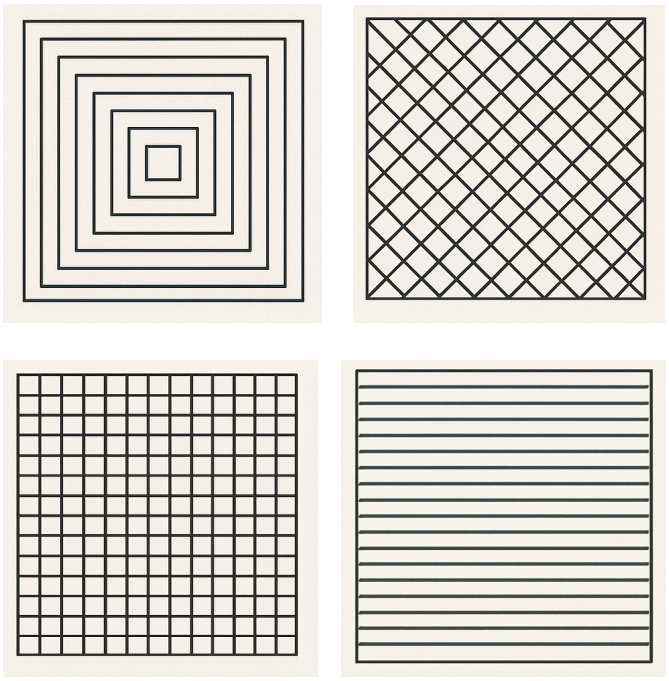

Figure 3-7 Infill patterns top left to bottom right (concentric, rectilinear 45°, rectilinear 0°, aligned rectilinear 0°)

3.4.1.3 Post Cooling

In semi-crystalline polymers such as PEEK, residual stresses and out-of-plane warp are governed by both thermal gradients during solidification and the crystallization kinetics that follow extrusion. Reviews focused specifically on FFF-printed PEEK emphasize that minimizing bed-to-ambient temperature differences (e.g., via a heated enclosure) is critical for dimensional stability, and that recommended practice is to control the chamber temperature rather than allow rapid, uncontrolled cooling [35]. Beyond the printing stage, classical thermoplastic-composite studies show that higher cooling rates reduce crystallinity and weaken interfacial properties: for CF-PEEK, increasing the cooling rate lowers crystallinity and bond strength [36]. Importantly, if the chamber temperature is turned off immediately after the end of the print, the uppermost layers have substantially less time to crystallize than those deposited earlier, leading to differences in crystallinity through the part thickness. That is why maintaining elevated temperatures post-printing is important to allow more uniform crystallization for the entire print and reduce internal stresses. These results motivated exploring controlled cool-downs after deposition to relieve gradients and promote more uniform crystallization.

Studies support two complementary principles for post-print management: first hold the environment warm enough to avoid steep through-thickness gradients while the part is semi-molten and crystallizing, and then second decrease temperature gradually so that crystallinity develops uniformly and residual thermal strain is not “frozen in.” In PEEK and it carbon reinforced variants specifically, the enclosure is often treated as a primary control variable to limit gradients, while post-process thermal control (annealing or cooling ramps) is used to tune crystallinity and dimensional stability [35].

- **Strategy A – Chamber only controlled cooling**

Our initial post-print strategy focused on holding the chamber at its initial temperature for 5 minutes and then gradually reducing the temperature in 5 °C steps every 5 minutes terminating at 150 °C, while the bed was turned off immediately. This hold point was chosen based on the known crystallization window of CF PEEK, which initiates near 280 °C and peaks between 180–200 °C. Maintaining chamber temperature above 150 °C allowed the part to complete most of its crystallization under uniform thermal conditions, minimizing internal thermal gradients and reducing differential shrinkage

- **Strategy B – Synchronized chamber and bed cooling**

To further minimize thermal gradients during post-print solidification, a synchronized cooling strategy was implemented. In this method, both the chamber and the build plate were cooled down simultaneously in 5 °C decrements every 5 minutes, starting immediately after print completion. The cadence and temperature drop were applied equally to both components to maintain uniform thermal conditions throughout the part volume. This approach was designed to mitigate temperature disparities between top and bottom layers, support uniform crystallization, and prevent differential contraction.

3.4.1.4 Design of Experiments

After identifying a stable cooling strategy and infill pattern, a structured Design of Experiments (DoE) was conducted to systematically investigate the effects of key thermal parameters on the flatness and dimensional stability of CF-PEEK prints.

The factors were chosen due to their direct influence on interlayer adhesion, residual stress, and crystallization kinetics, all of which significantly affect the warping tendency in high-performance polymer FFF. The selection of factor levels for the Box-Behnken experimental design was based on a combination of material datasheets, equipment limitations, and preliminary single-variable tests.
For chamber temperature, the lower level of 210°C was chosen as a conservative minimum for PEEK-class materials, sufficient to maintain partial crystallization control without excessive heat buildup. The upper limit of 300°C represents the highest stable chamber condition achievable with the equipment.
The selected range (240°C to 280°C) for bed temperature encompasses the lower bound required for CF PEEK to adhere securely to the building plate (typically >230°C) and approaches the upper practical limit for maintaining stable geometry without risking overheating and sticking the layers too much to the build platform.
The chosen range of 280°C to 360°C of the layer heater reflects the distinct melting and degradation profiles of CF PEEK and LDS PEEK. The lower limit of 280°C is near the minimal extrusion temperature at which LDS PEEK can be reliably printed. The center point of 300°C was selected as a moderate value to facilitate both material deposition and avoid signs of thermal degradation. The upper bound, 360°C, pushes the toward the maximum safe range.

Table 3-5: Design of Experiments factors for CF PEEK

Parameter	**Level -1 (Low)**	**Level 0 (Center)**	**Level +1 (High)**
Chamber Temperature (°C)	210	265	300
Bed Temperature (°C)	240	260	280
Layer Heater (°C)	280	300	360

3.5 Phase 2 – Dual material printing (CF & LDS PEEK)

Prior to dual-material testing, LDS-PEEK was printed independently to evaluate its printability conditions. Manufacturers recommended parameters were adapted to the FFF machine characteristics. Key settings included a nozzle temperature of 445 °C, chamber temperature of 280 °C, and bed temperature of 260 °C. These standalone prints served as a process reference for evaluating compatibility with CF-PEEK during subsequent dual-material experiments.

Table 3-6: LDS PEEK printing parameters

Parameter	Value
Extruder temperature (°C)	455
Bed temperature (°C)	260
Chamber temperature (°C)	285
Layer heater (°C)	300
Infill density (%)	100

3.5.1 Dual material printing workflow

All of the dual-material prints were fabricated in a single sequential process divided into 2 steps:

1. CF-PEEK Base: A 70 × 70 mm CF-PEEK panel was printed using the optimized baseline settings from Phase 1.
2. LDS-PEEK Deposition: After completion of the base, the print is paused while the chamber and bed temperatures were maintained to preserve heat. The CF-PEEK filament was replaced with LDS-PEEK, the nozzle temperature was increased to 445 °C, and the chamber temperature was raised to 285 °C before resuming the print to accommodate for LDS PEEK requirements.

The process relies on single extrusion mechanism.

3.5.2 Design of Experiments

Preliminary prints suggested that dimensional stability in dual-material parts is not solely dependent on material choice, but also on geometric and process parameters. Unlike CF-PEEK alone, which performed best with unidirectional aligned infill, early dual-material parts exhibited increased warping when the same infill strategy was used. Furthermore, the warping behavior changed along changes in layer height, and number of LDS PEEK layers as well.

A full-factorial design was used to evaluate all combinations of the three factors at three levels each. The experimental matrix was generated using Design Expert software. Each print used the same geometry and maintained the chamber and bed cooling strategy defined in Phase 1, infill type was chosen to be rectilinear.

Table 3-7: Design of Experiments factors for LDS PEEK

Parameter	Level -1 (Low)	Level 0 (Center)	Level +1 (High)
Layer height (mm)	0.125	0.175	0.25
Number of LDS layers	1	2	3

Raster angle (°)	0	20	45

The layer height varied between 0.125 mm and 0.25 mm; with 0.125 mm being near the minimum required height of functional LDS PEEK. The number of LDS layers (1 to 3) was chosen to simulate different functional top-layer thicknesses. The infill orientation is rectilinear with different raster angles ranging 0° to 45° to capture the behavior in different filament deposition orientation and how that affects stress accumulation.

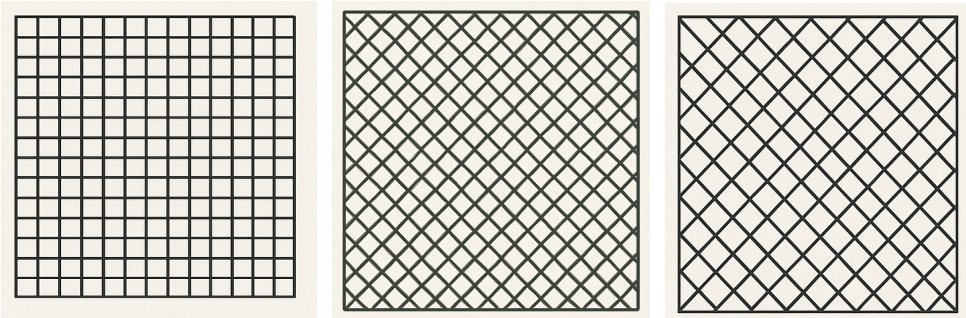

3.6 Interlayer bonding

For interlayer bonding analysis, cross-sections of the printed specimens were prepared. Samples were cut perpendicular to the build plane using a precision diamond saw to avoid introducing thermal damage or deformation. The cut surfaces were mounted in epoxy and progressively polished using SiC abrasive papers down to 1200 grit, followed by fine polishing with diamond suspension to achieve a smooth surface suitable for microscopy. For SEM imaging, samples were sputter-coated with a thin platinum layer to improve surface conductivity and prevent charging. Imaging was carried out at 5–15 kV acceleration voltage with magnification up to 5000 to reveal both interlayer contact and potential voids at the material interface.

Figure 3-8: Samples for microscope analysis

4 Results and Discussion

4.1 Phase 1 – Printing of CF PEEK

4.1.1 Effect of Infill Pattern

Infill pattern is found to have a high impact on warping; across otherwise identical printing settings, different infills (concentric, rectilinear 45°, rectilinear 90° and aligned rectilinear at 0°) resulted in varying outcomes (Figure 4-1).
As seen from the sample prints, strong edge lifting and various bowing behaviors were present. However, the default aligned rectilinear at 0° pattern visibly helped in reducing both issues and resulted in somewhat repetitive pattern unlike the other types where it was not possible to narrow down the behavior. While downside warp was still visible, it still presented a good window opportunity for future improvement unlike the other patterns.

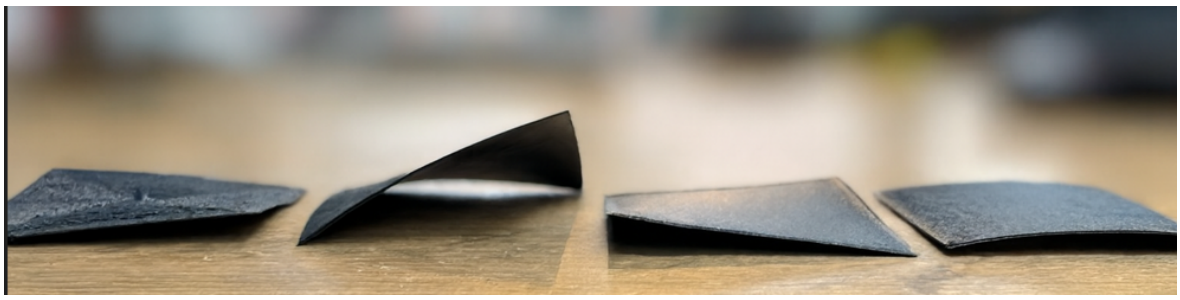

Figure 4-1: Print results from different infills

The warp deviation deviations on the printed parts with different infills can be seen through distortion maps;

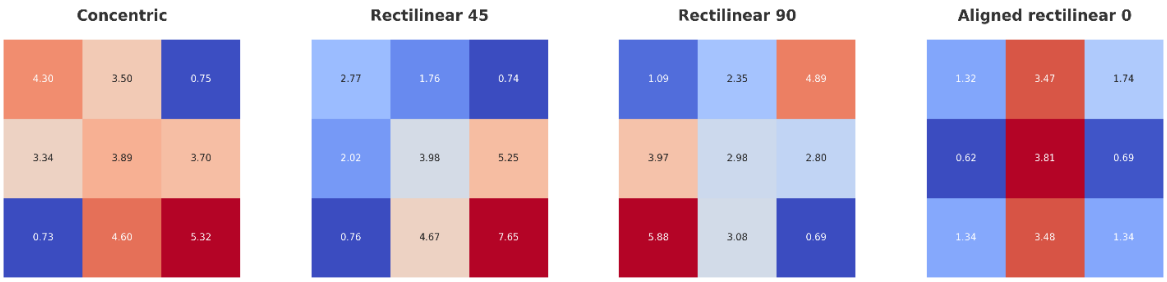

Figure 4-2: Distortion map of the different infills

Table 4-1: Results from different infill orientations

Trial	**Topology**	**Raster angles (°)**	**Adhesion notes**	**Std (mm)**	**Decision**
T-01	Concentric	n/a	Edge lifting	1,597	Reject
T-02	Rectilinear	45	High internal stress along diagonals	2,301	Reject
T-03	Rectilinear	90	Improved stress distribution	1,666	Reject
T-04	Aligned Rectilinear	**0**	OK, more uniform flatness	1,256	**Keep**

After the initial round of testing, aligned rectilinear pattern at 0° produced the most optimal results, so it was selected as the standard infill for the remaining experiments.
While there is a scarcity of research focusing specifically on infill influence on CF-PEEK FFF printing, the decision to fix this infill topology for all subsequent experiments is still consistent with the literature on PEEK, it is reported that 0° raster offer better on-axis stiffness and interbed consolidation; traits that correlate with reduced bending and distortion in thin plates [37]. Raster orientation is a key parameter in shaping the response of semi-crystalline PEEK; 0° layups are widely adopted as stable baselines, in tandem with elevated chamber temperatures to reduce thermal gradients and crystallization-induced shrinkage [35]. More generally across polymers, it is well proven that the deposition angle explicitly influences dimensional deviations, empirically confirming that toolpath orientation measurably affects shape error and thus should be controlled before modelling thermal effects [38]. Other reviews of extrusion additive manufacturing further emphasizes the tight coupling between path planning (including raster orientation) and distortion, reinforcing the methodological choice to lock the toolpath and then use design of experiments to study factors that directly govern residual thermal strain; namely chamber and cooling temperatures, and the post-print cooling ramp [39]. Taken together, our pilot tests and the cited evidence support treating aligned rectilinear as the controlled baseline for thin CF-PEEK plates. This removes a major source of variance, aligns with best practices for CF-PEEK, and allows the DoE to isolate and optimize the thermal conditions that most strongly determine warp.

4.1.2 Effect of cooling strategy

The 'chamber only' cooling strategy produced only partial improvement in flatness: bottom layers contracted too early as they were rapidly cooled by the unheated bed, while the upper layers, still exposed to a warm chamber, remained hot. Downward warping persisted and was heavily noticeable on the coupons.

To quantify the gradient, we monitored surface temperatures from the top and bottom faces using an IR camera during the step-down sequence. Figure 4-4 plots the measured temperatures of the top and bottom surfaces versus chamber set-point. As the chamber decreased from 300 °C to 200 °C, the top surface trailed the set-point only modestly, while the bottom surface, in contact with the cooling bed dropped much faster, creating a disparity that reached ≈ 40 °C. This top–bottom temperature gap implies uneven crystallization and differential thermal contraction through the thickness. These data confirmed that chamber-only stepping is insufficient; the bed must be controlled in order to avoid locking-in gradients.

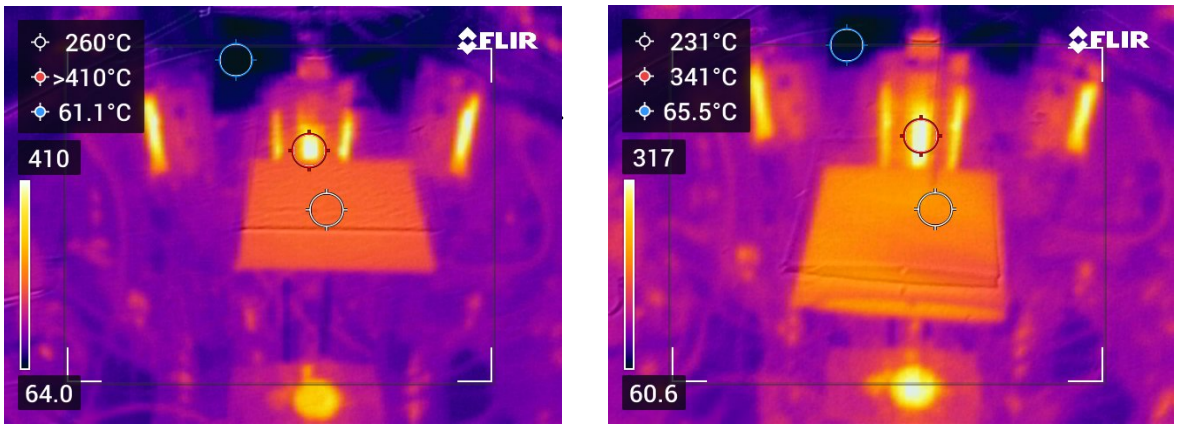

Figure 4-3: Example of infrared camera observations for top and bottom faces

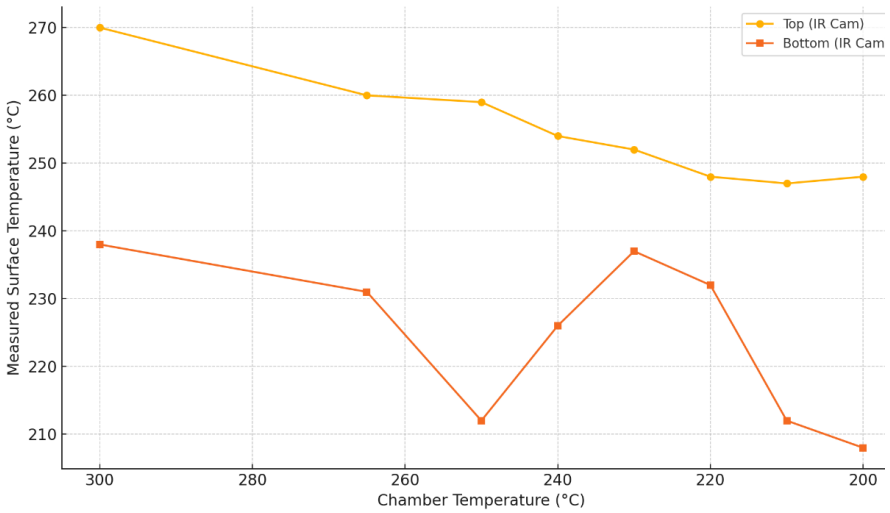

Figure 4-4: Temperature across the part when chamber is cooling

The introduction of the synchronous ramp (i.e: simultaneous cooling of the bed and chamber), helped with a uniform temperature decay across the part, and coupons exhibited significantly reduced warping. This result aligns with guidance to reduce temperature differentials in PEEK FFF by controlling the enclosure and overall thermal history [35] and with composite literature showing that moderated cooling rates lead to more uniform crystallinity and improved stability [40]. We therefore adopted the synchronous cooling method for both the chamber and the bed as the baseline cooling strategy for all subsequent experiments.

Table 4-2: Comparison between different cooling procedures

Metric	**Chamber Cooling**	**Chamber + Bed Cooling**	**Improvement**
Max z-deviation (mm)	3.83	1.74	Improved by ~ 55%
Standard Deviation (mm)	1.14	0.46	Improved by ~ 60%
Visual Flatness	Downard curvature	Flatter, curvature still present	

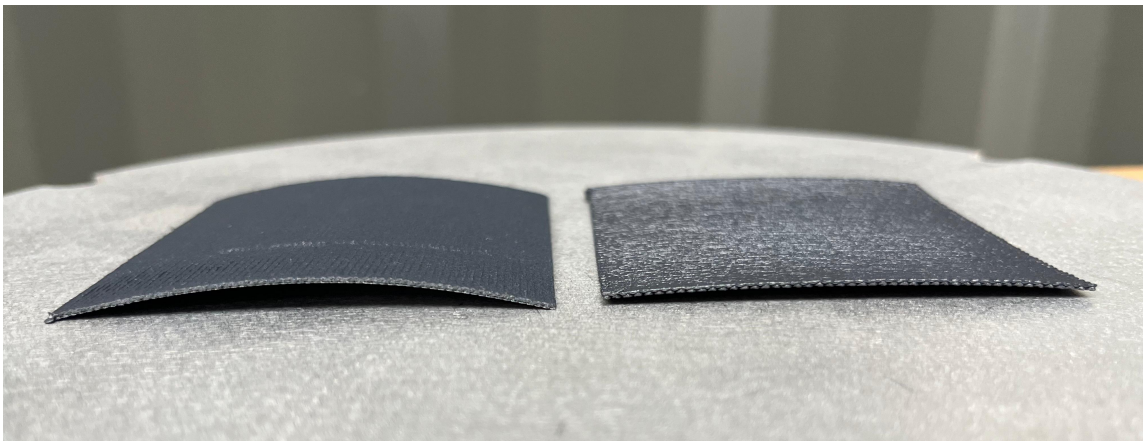

Figure 4-5: Print with chamber cooling (left), print with synchronous cooling (right)

To further confirm our experimental results and the importance of post-print cooling, an ANSYS thermal simulation was performed. The results showed same trend; post-cooling dramatically reduces warpage. While predicted and measured magnitudes were slightly different, the numerical model still successfully captured the physical mechanism.

Table 4-3: Ansys simulation settings for CF PEEK

Category	Input
Geometry	70 × 70 mm panel; thickness = 0.7 mm
Software	ANSYS Mechanical
Material properties	Density, thermal conductivity, specific heat, elastic modulus, Poisson's ratio
CTE (Z-direction)	CF-PEEK: 45–93 × 10^{-6} K^{-1}
Glass transition (Tg)	~150 °C
Extruder temperature	435 °C
Chamber temperature	300 → 150 °C
Bed temperature	265 °C
Cooling strategy	Chamber-only (natural) vs. controlled ramp (5 °C decrease every 5 min)
Constraints	Base face fixed (to simulate adhesion to build plate)
Outputs recorded	Maximum Z-direction displacement

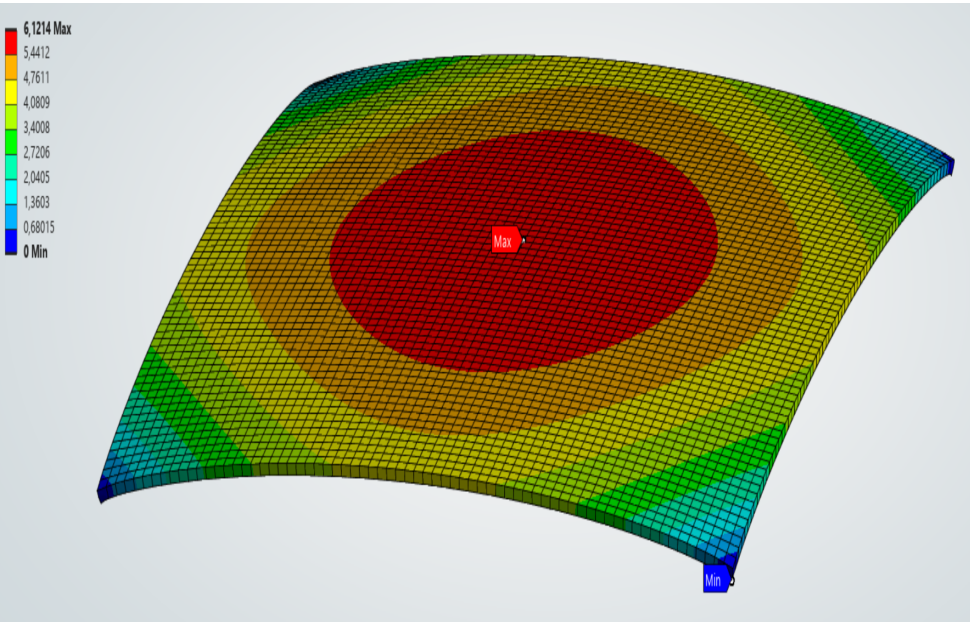

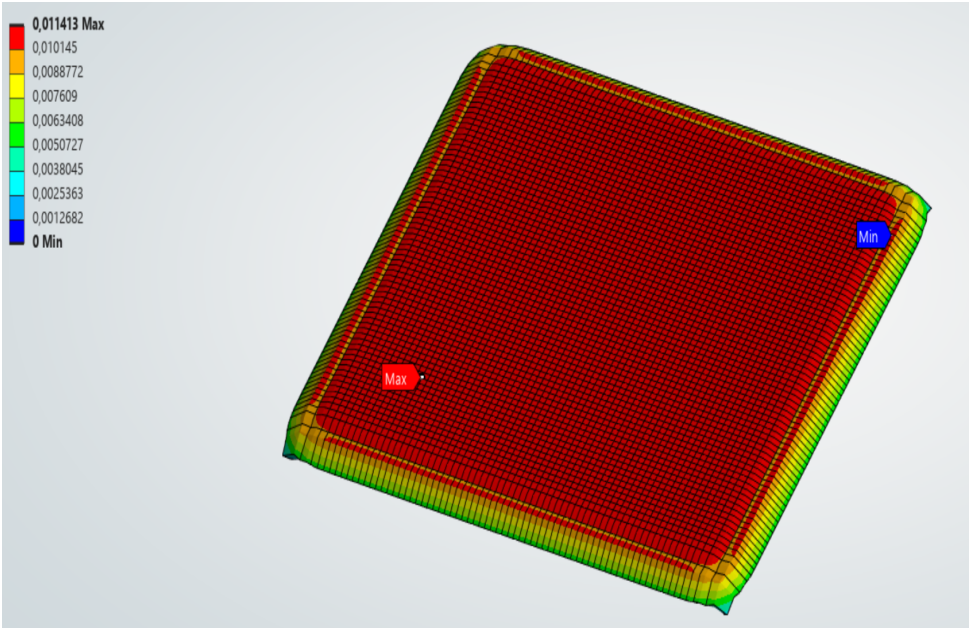

Figure 4-6: Directional deformation (mm) of panel without cooling, panel with ramped cooling process

The simulation was slightly overpredicted but captured the same trend: significant deformation reduction with controlled post-cooling. The differences in experimental versus simulation results are due to CF-PEEK panel being modeled using homogenized thermo-mechanical properties whereas in reality, PEEK undergoes phase transitions during cooling, which change its modulus and shrinkage behavior. Additionally, the simulation assumed isotropic bulk properties with no consideration to the carbon fiber alignment along the deposition path.

These simplifications tend to overpredict deformation in some directions while underpredicting others., but they still gave us an idea on the importance of post cooling processes

4.1.3 Analysis of variance evaluation

4.1.3.1 Flatness deviation

A total of 17 experimental runs were generated using Design Expert Software, including center point replications to estimate pure error and assess model fit. All other process parameters (Table 3-5) were held constant and the synchronous cooling of bed and chamber strategy was applied. The warping deviation measurements of the trials are presented below:

Table 4-4: Warp deviation results

STD	RUN	Z_deviation (mm)	standard deviation (mm)
17	1	1,74	**0,555958**
3	2	3,54	**1,111956**
8	3	4,33	**1,575266**
15	4	2,57	**0,791231**
10	5	4,7	**1,89595**
11	6	6	**2,054877**
1	7	2,72	**0,739641**
4	8	4,22	**1,407069**
7	9	2,84	**0,998755**
14	10	0,94	**0,287999**
12	11	4,01	**1,225574**
16	12	0,77	**0,226329**
9	13	2,08	**0,583705**
6	14	3,89	**1,262459**
13	15	0,56	**0,186375**
2	16	2,6	**0,869585**
5	17	6,25	**1,809572**

Three analytical models were computed to evaluate the robustness and the regression models (Table 4-3); R-squared (R^2), Adjusted R-squared (Adj R^2), and Predicted R-squared while Adeq Precision measures the signal to noise ratio.
R^2 reveals how well the model explains the variance in mechanical strength, a greater R^2 suggests a stronger correlation between input parameters and responses. The Adj R^2 prevents overfitting by taking into consideration the number of predictors. And finally, predicted R^2 is indicative of the model's capacity to predict data.

Table 4-3: Model fit summary table

R^2	0.6633
Adjusted R^2	0.4613
Predicted R^2	0.3087

Adeq Precision	4.2392

The R^2 value of 0.6633 means there is a moderate link between process settings and results. While not a very high, it is considered reasonable when dealing with additive manufacturing especially in warp of semi-crystalline materials. Warping is stochastic and influenced by a mix of thermal and mechanical effects that interact in a non-linear way. Past research has also reported similar outcomes; for instance, predictive models for height shrinkage for ABS parts in fused deposition modeling (FDM) reported R^2 value of 0.622 [41]. Another study evaluating the effect of part size, infill density and layer thickness on dimensional accuracy reported R^2 value of 0.6704 [42].

The Adequate precision is higher than 4, and the predicted R^2 of 0.3087 is in reasonable agreement with the Adjusted R^2 of 0.4613; the difference is less than 0.2.

Table 4-4: Analysis of variance table

Source	Sum of Squares	df	Mean Square	F-value	p-value	Contribution (%)
Model	2.51	6	0.4178	3.28	0.0472	66.40
A – Chamber T	0.0013	1	0.0013	0.0101	0.9218	0.03
B – Bed T	0.1182	1	0.1182	0.9286	0.3579	3.13
C – Layer Heater T	0.0006	1	0.0006	0.0044	0.9482	0.02
A^2	0.6337	1	0.6337	4.98	0.0497	16.76
B^2	0.7206	1	0.7206	5.66	0.0386	19.07
C^2	0.7406	1	0.7406	5.82	0.0365	19.59
Residual	1.27	10	0.1272			33.60
Cor Total	3.78	16				100.00

Through examination of the results, the linear effects of the chamber, bed and layer heater temperatures are not significant. Whereas the quadratic effects of these parameters (A^2, B^2, C^2) are highly influential. These quadratic terms mean that there's a curved response surface; flatness deviation is not directly influenced by a simple increase or decrease in the three factors but rather sensitive to non-linear effects of the bed, layer heater and chamber temperatures. The optimal flatness doesn't occur at extremes, but at intermediate values.

This behavior is consistent with previous findings on residual stresses and warpage in FFF-printed composites, which highlight bed temperature as a primary factor influencing deformation in fiber-reinforced thermoplastics [43]. Moreover, research on CF-PEEK

demonstrates a trade-off between printing efficiency and dimensional accuracy, emphasizing the necessity of optimizing process parameters in high-temperature polymer [35]. Altogether, these results indicate that minimizing flatness deviation in CF-PEEK requires a precise calibration of thermal inputs to achieve an optimal balance. Rather than arbitrarily increasing temperatures, careful control is important to manage residual stress development.

$$\begin{aligned}\text{Flatness deviatiation} &= -122.98677 + 0.099533\text{A} + 0.576939\text{B} \\ &+ 0.237735\text{C} - 0.000195A^2 - 0.001121B^2 \\ &- 0.000372C^2\end{aligned} \tag{4.1}$$

Based on the experimental data and surface response modelling, the optimal process window for minimizing flatness deviation in CF-PEEK panels was identified to be approximately 255 °C for chamber temperature and 257 °C for bed temperature. Operating within this range resulted in significantly reduced warping and dimensional distortion. Conversely, reducing either the chamber or bed temperature below this window led to the development of thermal gradients between the top and bottom layers of the print, causing increased residual stress and warpage. This behavior is consistent with findings from Zhang et al. [44] , who developed a warp deformation model for carbon fiber-reinforced PEEK and demonstrated that lower chamber temperatures increase shrinkage stress and deformation due to insufficient thermal balance. In addition to confirming that the temperature difference between the bed and the chamber during printing and cooling should be reduced as possible to decrease warping deformations.

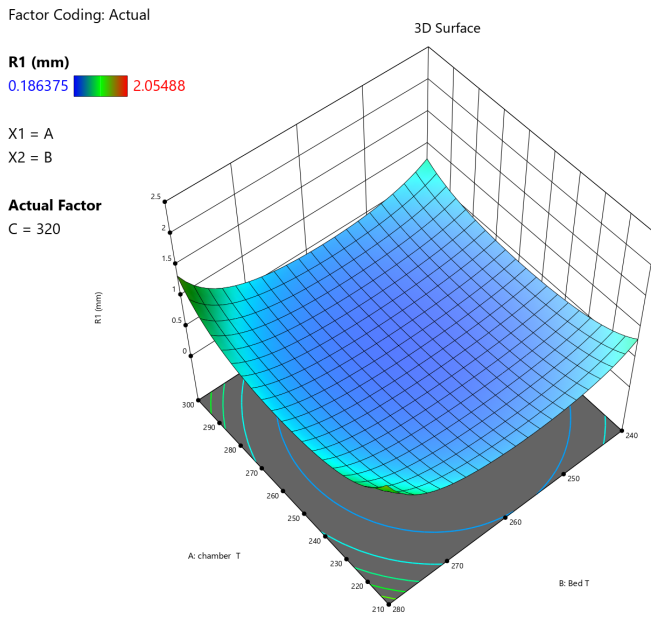

Figure 4-7: Response surface plot for warpage deviation

The response surface plot (Figure 4-7) illustrates the combined effect of chamber temperature (A) and bed temperature (B) on flatness deviation, with the layer heater temperature (C) fixed at 320 °C. The plot reveals a distinct minimum region at intermediate chamber and bed temperatures, where flatness deviation is reduced to approximately 0.18 mm. Deviation increases at both lower and higher extremes, highlighting the existence of an optimal temperature window rather than a linear trend.

Overall, the combination of ANOVA, regression modeling, and response surface analysis demonstrates that dimensional flatness of CF-PEEK parts in FFF printing is optimized at moderate chamber and bed temperatures, while excessive or insufficient values increase deviation. Thus, a carefully controlled thermal environment where the thermal gradient experienced by the print is kept at minimum is essential for producing flat, dimensionally accurate CF-PEEK parts. The less thermal gradient difference there is between bed and chamber the more the part is stable.

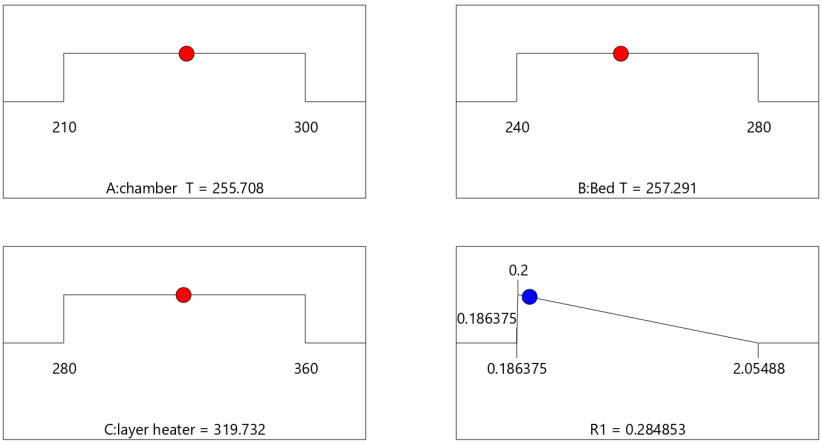

Figure 4-8: Suggested printing window to minimize warp

4.1.3.2 Dimensional accuracy

In this measurement phase by using vernier caliper, the thickness of each sample is measured at 3 different locations and averaged, the deviation from the target 0,71 mm is then calculated. The respective measurements are shown in table 4-9.

Table 4-5: Dimensional deviation results

Chamber T (°C)	Bed T (°C)	Layer heater (°C)	Thickness deviation (mm)
260	265	300	0,0045
210	280	300	-0,053

300	265	360	-0,042
260	265	300	-0,0075
260	280	280	0,0154
260	240	360	-0,0195
210	240	300	0,0201
300	280	300	-0,05
210	265	360	-0,0392
260	265	300	-0,01
260	280	360	-0,0634
260	265	300	0,004
260	240	280	0,0209
300	265	280	0,023
260	265	300	-0,014
300	240	300	0,0114
210	265	280	0,0209

The following part presents the statistical analysis which provides insights into the parameters' interactions and how they affect the thickness.

Table 4-7: Model fit summary table

R^2	0.8733
Adjusted R^2	0.8311
Predicted R^2	0.6857
Adeq Precision	16.4130

The Predicted R^2 of 0.8733 is in reasonable agreement with the Adjusted R^2 of 0.8311 (the difference is less than 0.2).

The equation of the final factors is represented in the following form:

$$\text{Thickness deviation} = -0.629262 + 0.028035B - 0.009153C - 0.000037B^2 + 0.000013C^2 \quad (4.2)$$

Table 4-8: Analysis of variance table

Source	Sum of Squares	df	Mean Square	F-value	p-value	Contribution (%)
Model	0.0120	4	0.0030	20.68	<0.0001	87.59
B – Bed T	0.0042	1	0.0042	29.23	0.0002	30.66
C – Layer Heater	0.0075	1	0.0075	51.58	<0.0001	54.74
B^2	0.0008	1	0.0008	5.41	0.0384	5.84
C^2	0.0009	1	0.0009	6.38	0.0266	6.57
Residual	0.0017	12	0.0001			12.41
Lack of Fit	0.0015	8	0.0002	2.57	0.1890	10.95
Pure Error	0.0003	4	0.0001			2.19
Cor Total	0.0137	16				100.00

The analysis indicated that layer heater temperature exerts the most significant impact on thickness accuracy of the prints with a domination of the linear effect. This dominance highlights the critical role of interlayer thermal heating as it decreases the presence of voids and enhances the overall density of the print as the gaps become smaller, however this also drives the part to become thinner than intended, particularly when dealing with thin parts below 1 mm. The enhanced consolidation of the material at excessive temperatures can promote high compaction of the deposited filament leading to a reduction in the final part.
In addition, the bed temperature also contributes to around 30% to the variation. Figure 4-9 indicates that at layer temperature of 320 °C, the deviation remains closest to zero around lower temperatures ~ 240 °C and becomes increasingly negative toward 280 °C leading to slightly thinner parts.

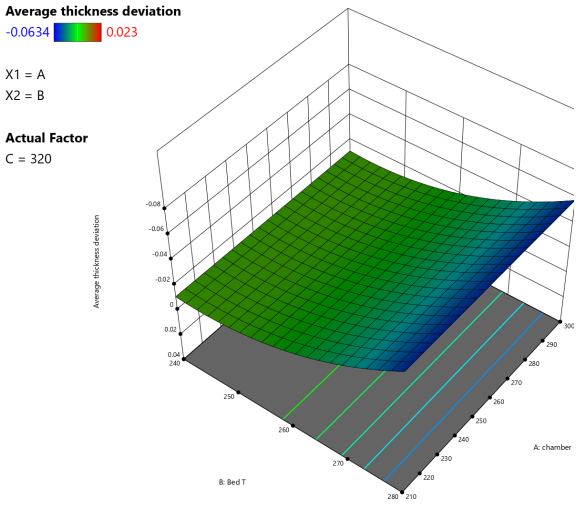

Figure 4-9: Surface Response plot

Taken together, these results demonstrate that dimensional accuracy in the Z-direction is governed primarily by the layer heater temperature, which drives systematic thinning at moderate to high settings, while bed temperature for the most part helps in maintaining the deviation at minimum around 200 °C – 270 °C and further reinforces the thinning effects at 280 °C and above. The quadratic contributions highlight that both parameters act nonlinearly, and that an optimal thermal window is essential to balance bonding, density, and dimensional fidelity.

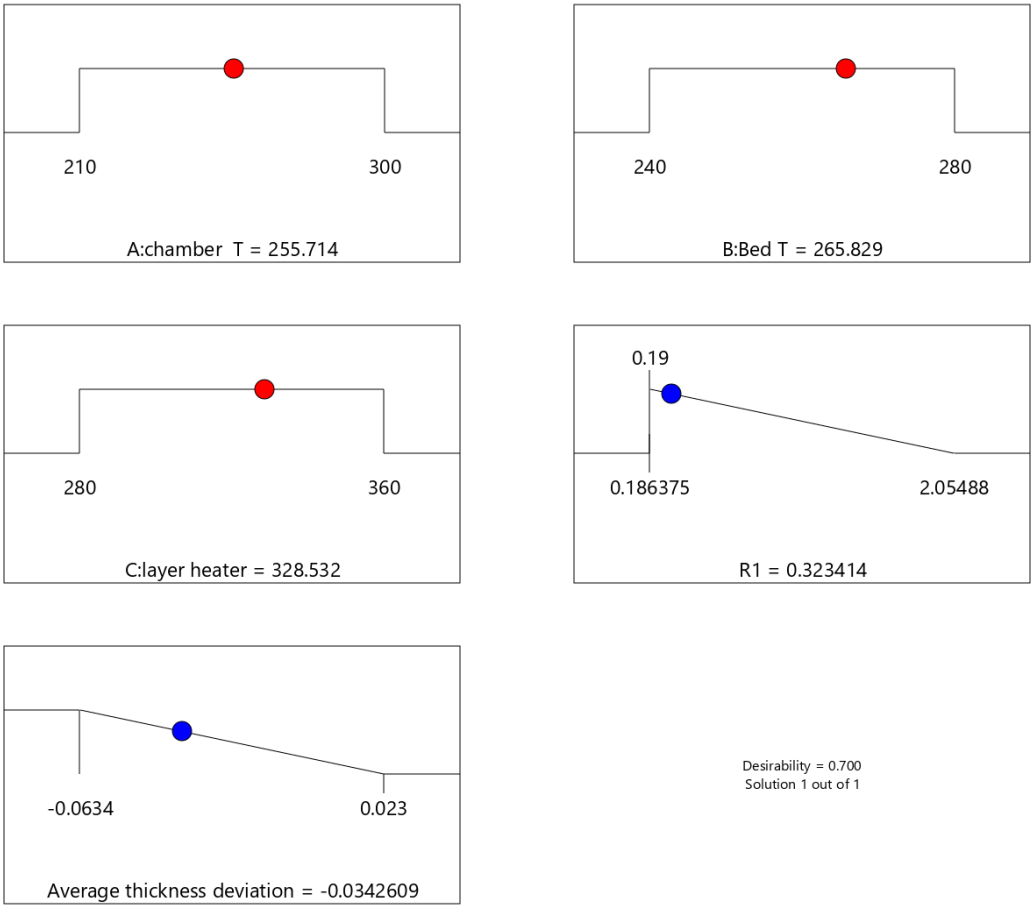

Figure 4-10: Suggested printing parameters for CF parameters

The final optimized thermal window suggested by the ANOVA analysis (chamber ≈ 256 °C, bed ≈ 266 °C, layer heater ≈ 329 °C) highlights the importance of maintaining low thermal gradients between the bed and chamber to control both flatness deviation and dimensional accuracy. Carbon fiber reinforcement significantly alters the crystallization behavior of PEEK blends, making precise thermal management essential for achieving adequate consolidation and dimensional stability. The analysis revealed that the layer heater exerts the strongest influence, dominating Z-direction dimensional accuracy by governing interlayer diffusion, void reduction, and overall part density. This observation is consistent with the impact of Orion's technology, where localized heating eliminates

cold joints and produces dense, fully bonded structures, while its absence leads to weak adhesion and void formation. At the same time, the chamber and bed temperatures provide secondary but necessary support by reducing shrinkage, relieving residual stresses, and stabilizing the base layers; factors directly linked to flatness and warpage control. The results converge on the conclusion that interlayer heating is the primary driver of thickness stability in CF-PEEK, while the combined contribution of chamber and bed temperatures ensures dimensional fidelity by mitigating distortion and enhancing adhesion across the build.

4.2 Phase two – Printing of LDS PEEK

4.2.1 Initial LDS- PEEK printing observations

To evaluate the printability and behavior of LDS-PEEK, it was first printed as a standalone part. When printed on its own, and considering the manufacturer's recommendation and the feature of our printer, the parameters of printing were set as follows;

Table 4-6: Printing parameters of LDS PEEK

Parameter	**Value**
Extruder temperature (°C**)**	445
Bed temperature (°C**)**	260
Chamber temperature (°C**)**	285
Layer heater (°C**)**	300
Print speed (mm/s)	40
Infill density (%)	100
Flow rate (%)	100

Under these conditions LDS PEEK showed excellent surface finish, consistent infill lines, in addition to consistent flatness regardless of infill orientation and without the need of any annealing or post cooling processes.

Although no published studies specifically address FFF of LDS-PEEK, research on neat PEEK and CF-PEEK provides useful context. Pure PEEK is generally very prone to warping more so that CF-peek and requires careful tunning reduces residual stresses [11]. Earlier experiments showed that CF-reinforced PEEK warping behavior is sensitive to infill orientation and controlled printing environment with minimal temperature variations. On the contrary, LDS-PEEK exhibits very stable behavior, suggesting that its thermal and rheological characteristics (higher melt flow index of 77g/10 min) may facilitate better layer fusion and lower anisotropic shrinkage during solidification. Table (4-7) summarizes the findings between the 2 materials

Table 4-7: Comparison of Printing behavior CF PEEK vs LDS PEEK

Property	**CF-PEEK**	**LDS-PEEK**
Surface finish	Rougher surfaces, visible raster marks; fiber pull-out possible	Smooth, uniform finish; consistent surface quality
Warping	Highly sensitive to cooling strategy and infill orientation (0° unidirectional best)	Excellent flatness; negligible warping without annealing or post-cooling
Dimensional accuracy	Z-deviation reduced only under optimized cooling (chamber and bed ramp)	Maintains thickness accuracy under standard conditions
Process sensitivity	Requires high chamber temperature and gradual cooling to avoid delamination	Prints stably under standard manufacturer settings
Need for post-processing	Sometimes necessary (annealing or controlled cooling) to reduce residual stress	Not required; parts remained stable after printing
Literature context	Matches known issues in CF-PEEK: high thermal stresses, anisotropic shrinkage	No specific FFF studies exist; behavior closer to neat PEEK

Figure 4-11: LDS PEEK print

4.2.2 Dual-material printing

4.2.2.1 Interface behavior

Initial multi-printing of CF-PPEK and LDS grade PEEK revealed that warping is present and is pronounced when LDS infill is identical to the one of CF-PEEK (aligned rectilinear at 0°).
The deposition of LDS PEEK layers on top of CF PEEK resulted in high bowing phenomena (Figure 4-11) despite post cooling. This warping behavior in dual material printing is mainly explained by the mismatch of the coefficients of thermal expansion (CTE). PEEK reinforced with carbon fibers, exhibits lower and more anisotropic thermal expansion in comparison with LDS-PEEK, a non-reinforced filament with higher and more isotropic behavior.

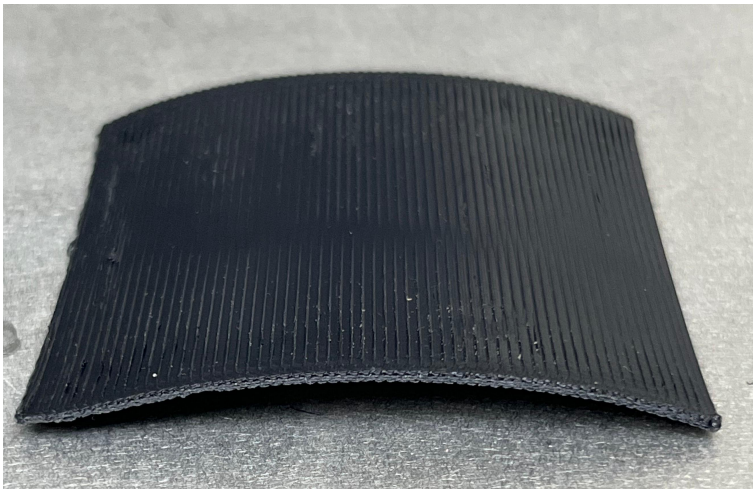

Figure 4-12: Multi-material print; LDS PEEK on top of CF PEEK (aligned infill)

As the prints cool, LDS-PEEK contracts more than the carbon reinforced substrate, primarily along the z-axis, creating significant tensile stresses. Comparison of the CTE values shows that in the flow direction, LDS PEEK expands more than CF-PEEK as it cools. However, in the transverse direction CF-PEEK has substantially higher expansion, so it contracts more strongly than LDS PEEK. The different shrinkage behavior causes an accumulation of internal stresses, which manifests as warping in our case. These behaviors align with classical thermomechanical incompatibility seen in dissimilar-material laminates. The following table summarizes typical CTE values of the two materials [33] [34]. Since CTE data for CF PEEK were unavailable, this comparison uses published values for CF30 (30 wt% carbon-fiber reinforced) as a reference. The CTE of PEEK decreases with fiber loading, so CF30 represents a lower-expansion limit, while CF10 is expected to fall between neat PEEK and CF30. Thus, using CF-PEEK 30 data therefore provide a conservative estimate of dimensional stability; in reality, CF10 will exhibit somewhat higher expansion, and thus greater potential for thermal mismatch and warpage.

Table 4-8: Coefficient of thermal expansion at 260 °C – 300 °C temperature range

Temperature Range (°C)	**LDS PEEK – Longitudinal (×10⁻⁶/K)**	**LDS PEEK – Transverse (×10⁻⁶/K)**	**CF-PEEK – Flow (×10⁻⁶/K)**	**CF-PEEK – Transverse (×10⁻⁶/K)**
23 – 100	18	26	–	–
50 – 100	–	–	9	44
100 – 150	–	–	6	46
150 – 200	–	–	14	93
200 – 260	46	67	–	–
260 – 300	63	88	–	–

Sun et al. [39] defines thermal strain using equation (4.3), a comparison between the 2 materials shows the difference and therefore explains the warping experienced

$$\varepsilon = \alpha.(T_g - T_c) \tag{4.3}$$

Where:

- α = thermal expansion coefficient of the material (1/K)
- T_g= glass transition temperature
- T_c= chamber temperature during printing

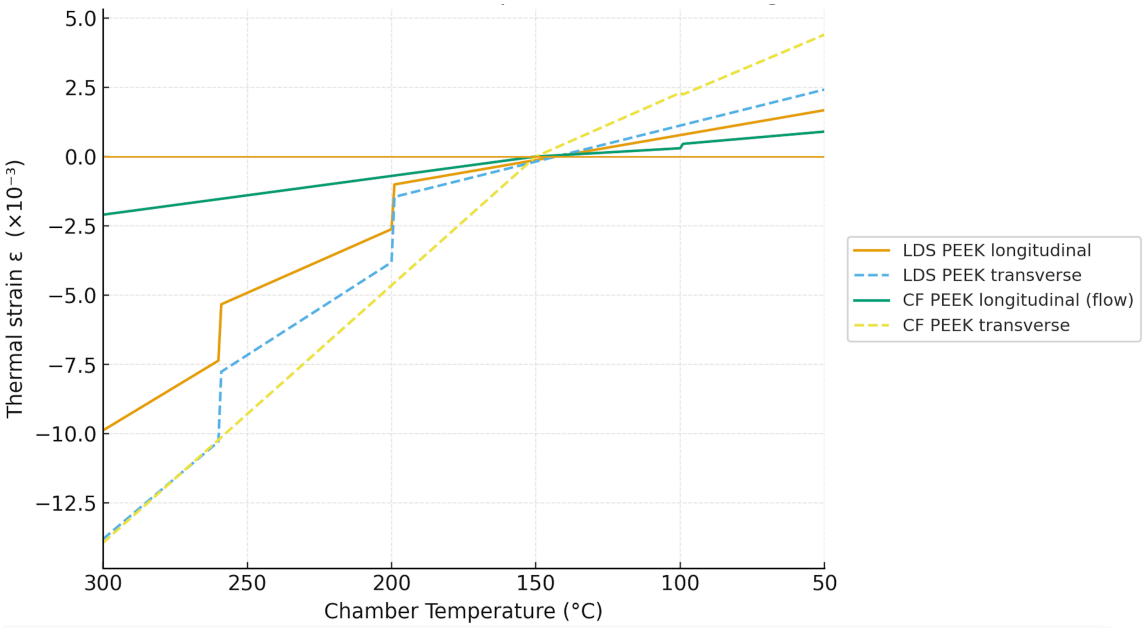

Figure 4-13: Thermal strain comparison LDS PEEK vs CF PEEK

In the longitudinal direction, LDS develops a larger tensile strain magnitude than CF-PEEK, indicating greater contraction of LDS on cooling. In the transverse direction, CF-PEEK's strain magnitude exceeds LDS; especially near and below glass transition temperature indicating greater transverse contraction of the CF substrate. The opposing dominance in the two principal directions evidences a biaxial CTE mismatch that is consistent with the observed warpage of the printed laminate during cool-down.

Another empirical model developed by Sun et al. [39] demonstrates that the magnitude of warp deformation (L_k) is proportional to the product of thermal expansion coefficient (α), temperature difference (ΔT), and the square of part thickness (nh), described by the relation:

$$L_k = \frac{3.\alpha.\Delta T.(nh)^2}{4} \tag{4.4}$$

Where:

- L_k = bending deformation (mm)
- α = thermal expansion coefficient of the material (1/K)
- ΔT = temperature change during cooldown (°C)
- h = number of printed layers
- n = layer height (mm)

Hence, this paved the way for the selection of our influencing factors; number of layers, layer height and raster angle as thermal stress distribution is highly sensitive to infill orientation. It is critical not only to control thermal settings but to also consider these parameters

4.2.3 DoE Results and interpretation

4.2.3.1 Flatness deviation

Table 4-9: Flatness deviation results

A: Layer Height (mm)	B: Number of LDS Layers	C: Raster Angle (°)	Standard deviation (mm)
0.175	2	20	1.30
0.175	2	20	1.35
0.25	3	20	2.20
0.175	1	0	0.80
0.25	1	20	2.21
0.175	2	20	1.32

0.175	2	20	1.29
0.25	2	0	1.08
0.175	3	0	1.05
0.125	2	0	0.88
0.125	2	45	2.30
0.175	1	45	2.09
0.125	3	20	1.50
0.175	2	20	1.28
0.25	2	45	2.60
0.175	3	45	2.40
0.125	1	20	1.10

The following part presents the statistical analysis which provides insights into the parameters' interactions and how they affect the part warping

Fit Statistics

Table 4-10: Model Fit

R^2	0.9484
Adjusted R^2	0.9249
Predicted R^2	0.8412
Adeq Precision	20.7821

The is a reasonable agreement between Predicted R^2 and Adjusted R^2.
A ratio greater than 4 is desirable.

$$\text{Flatness deviation} = +2.34380 - 17.66346A - 0.471467B + 0.031094C + 59.41832A^2 + 0.147412B^2 \quad (4.5)$$

Table 4-11: Analysis of variance

Source	Sum of Squares	df	Mean Square	F-value	p-value	Contribution (%)
A – Layer Height	0.6666	1	0.6666	26.01	0.0003	12.20
B – Number of LDS Layers	0.1117	1	0.1117	4.36	0.0609	2.05
C – Raster Angle	3.94	1	3.94	153.78	<0.0001	72.13
A^2	0.2053	1	0.2053	8.01	0.0164	3.76
B^2	0.0917	1	0.0917	3.58	0.0851	1.68
Residual	0.2819	11	0.0256			
Cor Total	5.4619	16				

Raster angle is the most dominant factor affecting flatness deviation in the case of multi-material print of LDS PEEK on top of CF PEEK. The raster orientation governs anisotropic shrinkage and warpage in FFF printing due to directional and residual stresses. In this study, as a rule, stable flatness deviation was found to be at raster angle of 0° in a rectilinear infill pattern. The positive coefficient (+0.0311) further indicates that flatness deviation increases with higher raster angles, as the more oblique the orientation of the rectilinear infill gets (i.e. from 20° to 45°), the more stress imbalance leads to warping.
The layer height also has a significant influence with both a negative regression coefficient on the linear term and a positive effect on the quadratic term. This implies that reducing the layer height initially improves flatness but after a certain threshold below 0,125 mm, it could be too low to ensure minimal flatness deviation. Generally, very thin layers are prone to inducing residual stress within the part as they usually require multiple layers to build the part, thus requiring more heating and cooling cycles [45]. Similarly on the other hand, thicker layers above 0.25 mm can cause higher thermal gradients, resulting in higher deformation [33].

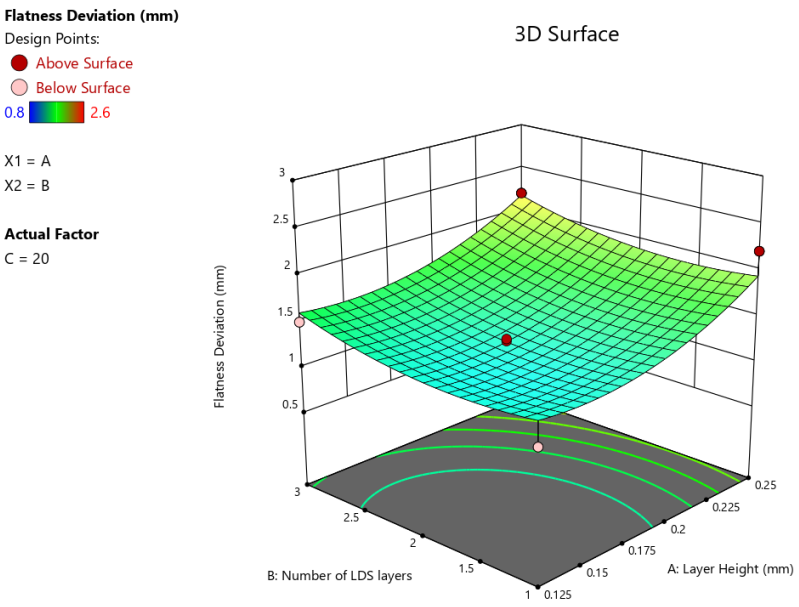

Figure 4-14: Surface response of flatness deviation

Figure (4-13) shows the fitted response surface of flatness deviation as a function of layer (A) height and the number of LDS layers (B), at a fixed raster angle of C = 20°. The shape of the contours indicates a stronger sensitivity to layer height than to the number of LDS layers: flatness deviation increases markedly with increasing A, while the effect of B is weaker and more gradual. The surface is gently convex, with the minimum predicted deviation located near the lower bounds of A and B; the highest deviations occur toward A ≈ 0.25 mm and B ≈ 3.

4.2.3.2 Dimensional accuracy

Table 4-12: Dimensional accuracy results

A: Layer Height (mm)	B: Number of Layers	C: Raster Angle (°)	% error deviation
0.175	2	20	5.78
0.175	2	20	6.25
0.250	3	20	12.40
0.175	1	0	3.26
0.250	1	20	11.57
0.175	2	20	5.94

0.175	2	20	6.20
0.250	2	0	8.07
0.175	3	0	3.57
0.125	2	0	0
0.125	2	45	2.28
0.175	1	45	6.43
0.125	3	20	1.31
0.175	2	20	6.08
0.250	2	45	14.93
0.175	3	45	7.40
0.125	1	20	0.76

The following part presents the statistical analysis which provides insights into the parameters' interactions and how they affect the dimensional accuracy along the z-axis.

Table 4-13: Model Fit summary

R^2	0.9960
Adjusted R^2	0.9936
Predicted R^2	0.9786
Adeq Precision	71.1000

$$\text{Thickness \% error} = -10.34015 + 67.34279A + 1.70483B + 0.011502C + 0.819497AB - 0.344060B^2 - 0.001562C^2 \quad (4.5)$$

Table 4-14: Analysis of variance results

Source	Sum of Squares	df	Mean Square	F-value	p-value	Contribution %

Model	269.66	6	44.94	416.28	< 0.0001	
A-Layer Height	233.36	1	233.36	2161.46	< 0.0001	86.19
B-Number of LDS layers	0.8637	1	0.8637	8.00	0.0179	0.32
C-Raster Angle	35.74	1	35.74	331.06	< 0.0001	13.20
AC	5.45	1	5.45	50.49	< 0.0001	2.01
B^2	0.4997	1	0.4997	4.63	0.0569	0.18
C^2	2.56	1	2.56	23.71	0.0007	0.95
Residual	1.08	10	0.1080			

The Model F-value of 416.28 implies the model is significant. There is only a 0.01% chance that an F-value this large could occur due to noise.
P-values less than 0.0500 indicate model terms are significant. In this case A, B, C, AC, $C^2$are significant model terms.

Dimensional error in the z-direction is primarily influenced by layer height; exhibiting a linear effect, the more it is increased the more there is deviation from nominal values. This effect is further intensified by the interaction of layer height and raster angle, as the error gets more amplified at larger raster angles. Thicker layers accumulate more stress and show worse dimensional accuracy, while reducing layer height increases mechanical strength and thermal diffusion, implying thinner stacks better resist deformation. Lower layer heights improve interlayer adhesion and reduce voids, leading to better dimensional fidelity.
The raster angle also showed a significant but nonlinear (concave) influence, where mid-range angles (~45°) introduced the highest errors, while boundary angles (0° or 90°) minimized deviation.

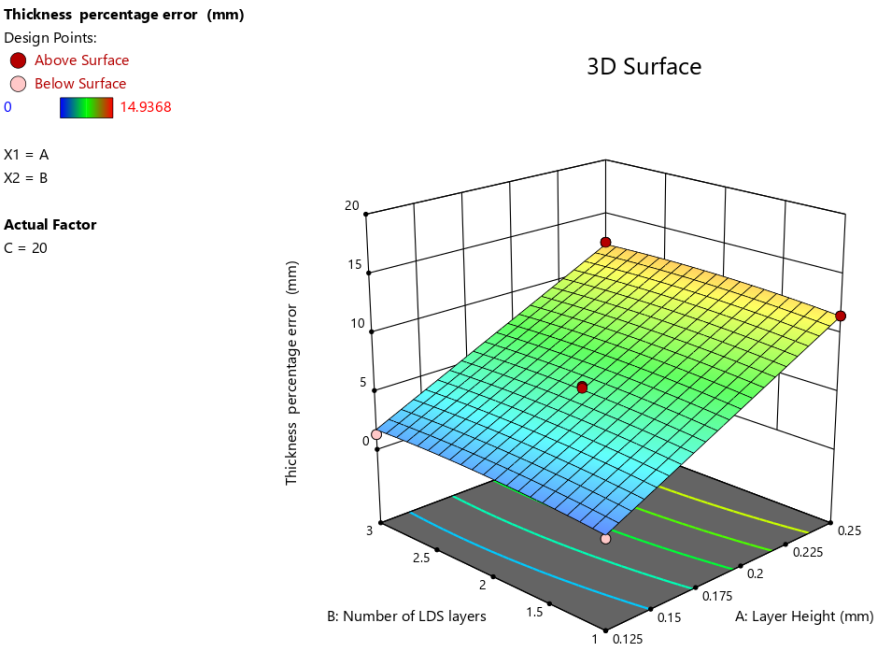

Figure 4-15: Surface response of error (%) thickness deviation

The 3D surface plot presents the strong impact of layer height (A) and the comparatively weaker effect of the number of LDS layers (B) on the percentage of thickness errors along the z-axis when printing LDS-PEEK on CF-PEEK. The error increases almost linearly with layer height, which confirms it as the primary contributor, while variations in the number of LDS layers only slightly impacts, with errors rising moderately at intermediate values. Overall, the plot demonstrates that minimizing dimensional error in the z-direction requires prioritizing low layer heights, while the number of LDS layers can be adjusted more flexibly without affecting accuracy severely.

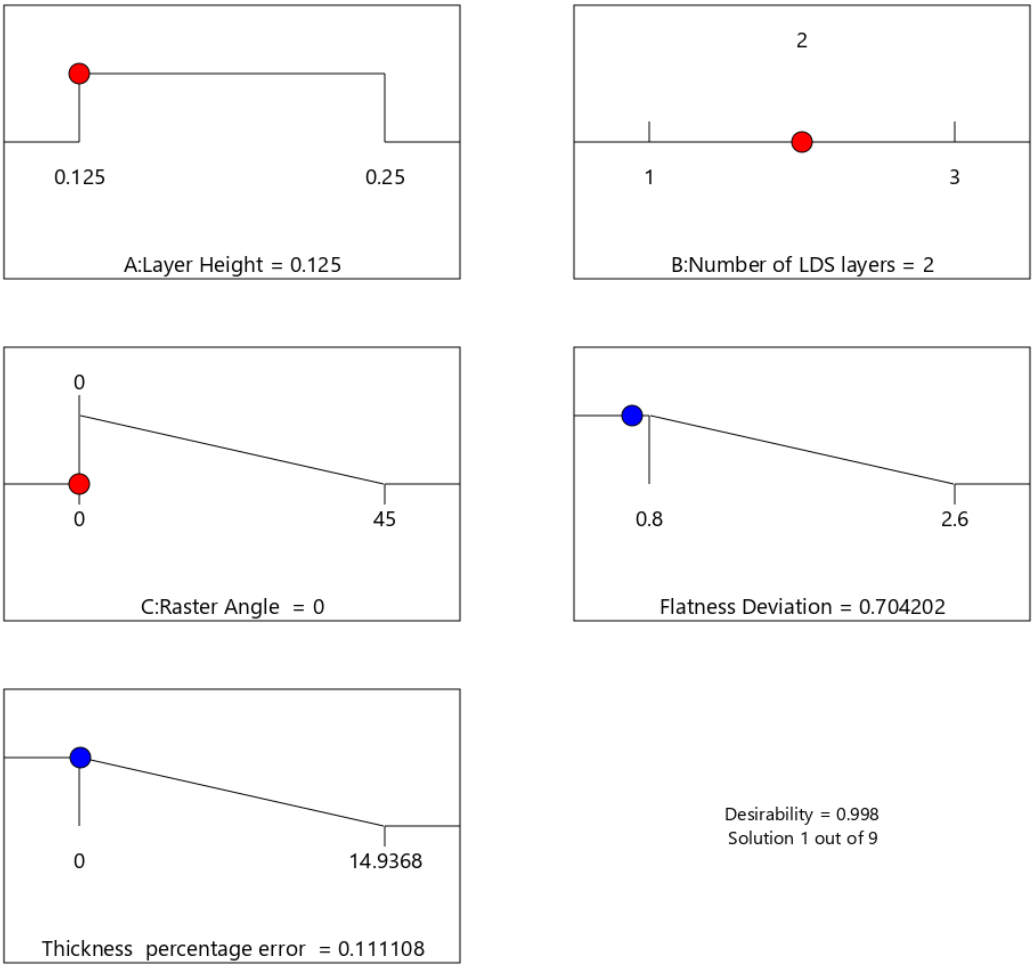

Figure 4-16: Optimized printing parameters for minimal flatness deviation and error (%) thickness

The optimization results identify the most suitable parameter combination for minimizing both flatness deviation and dimensional error in the multi-material printing of LDS-PEEK on CF-PEEK. The suggested settings are a layer height of 0.125 mm, two LDS layers, and a raster angle of 0°, which collectively yield a very low predicted thickness percentage error of 0.11% and a flatness deviation of 0.70 mm. The desirability function value of 0.998 confirms that this solution offers near-ideal conditions among the nine possible parameter sets evaluated. These results highlight that reducing layer height and maintaining a low raster angle are critical for achieving high dimensional accuracy, while the intermediate number of LDS layers balances structural requirements without introducing significant errors. This optimized combination provides a robust guideline for process parameter selection in fabricating dimensionally stable, multi-material FFF prints using LDS-PEEK and CF-PEEK.

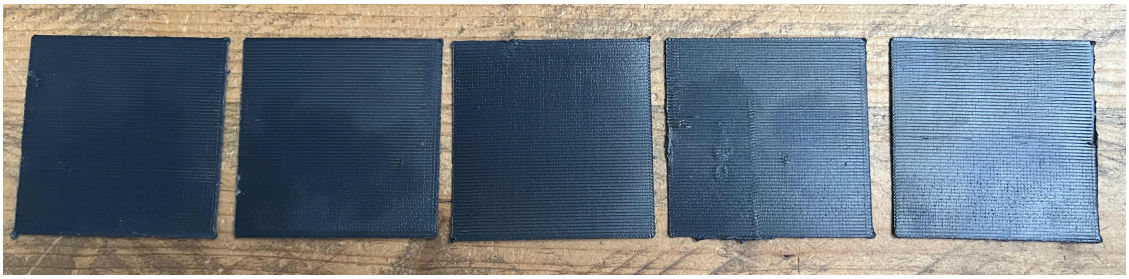

Figure 4-17: Confirmation runs with optimized parameters

The confirmation runs were performed at the predicted optimal settings. The model predicted a thickness error of 0.11%. The experimental confirmation runs yielded deviations of 0%, 0%, 0%, 0%, and 1%, resulting in an average thickness error of 0.2%. For flatness deviation, the predicted value was 0.70 mm, while the experimental mean was 0.49 mm, about 30% lower than predicted. This difference falls within the 95% prediction interval calculated by Design-Expert [46]. These results demonstrate great agreement between the predicted and experimental outcomes, thereby confirming the validity of the developed model for multi-material printing of CF PEEK and LDS PEEK.

4.2.4 Interlayer bonding

The optical microscopic analysis of the interlayer region between CF-PEEK and LDS-PEEK reveals a distinct yet continuous interface, confirming successful fusion of the two materials during the FFF process. Within the CF-PEEK matrix, carbon fibers are clearly visible, predominantly aligned along the printing direction, and in several cases extending towards the LDS-PEEK layer, which suggests localized mechanical interlocking and potential fiber bridging across the interface. The transition zone shows no evidence of large-scale delamination, indicating adequate thermal bonding between the dissimilar polymers.
Overall there is good fiber penetration into the LDS layer and continuous polymer transition without voids.

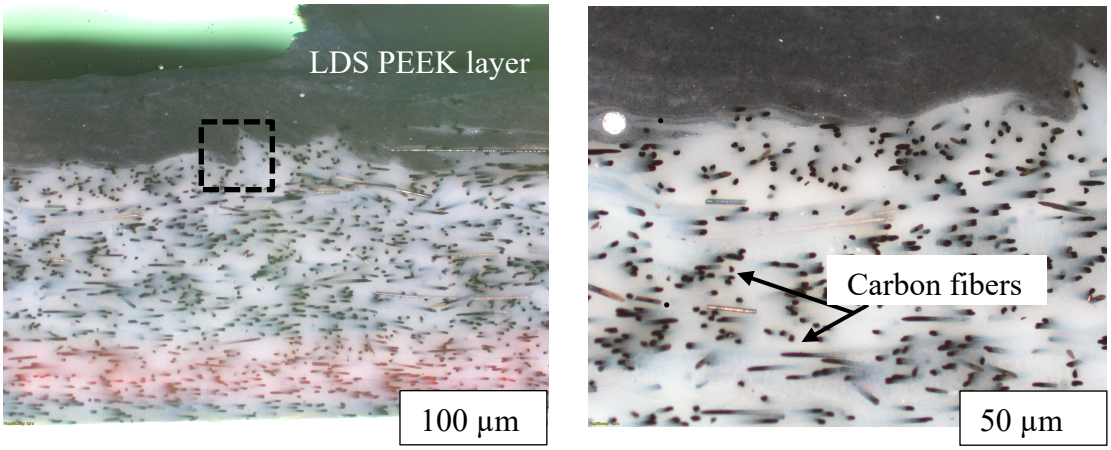

Figure 4-18: Cross section images of interlayer bonding

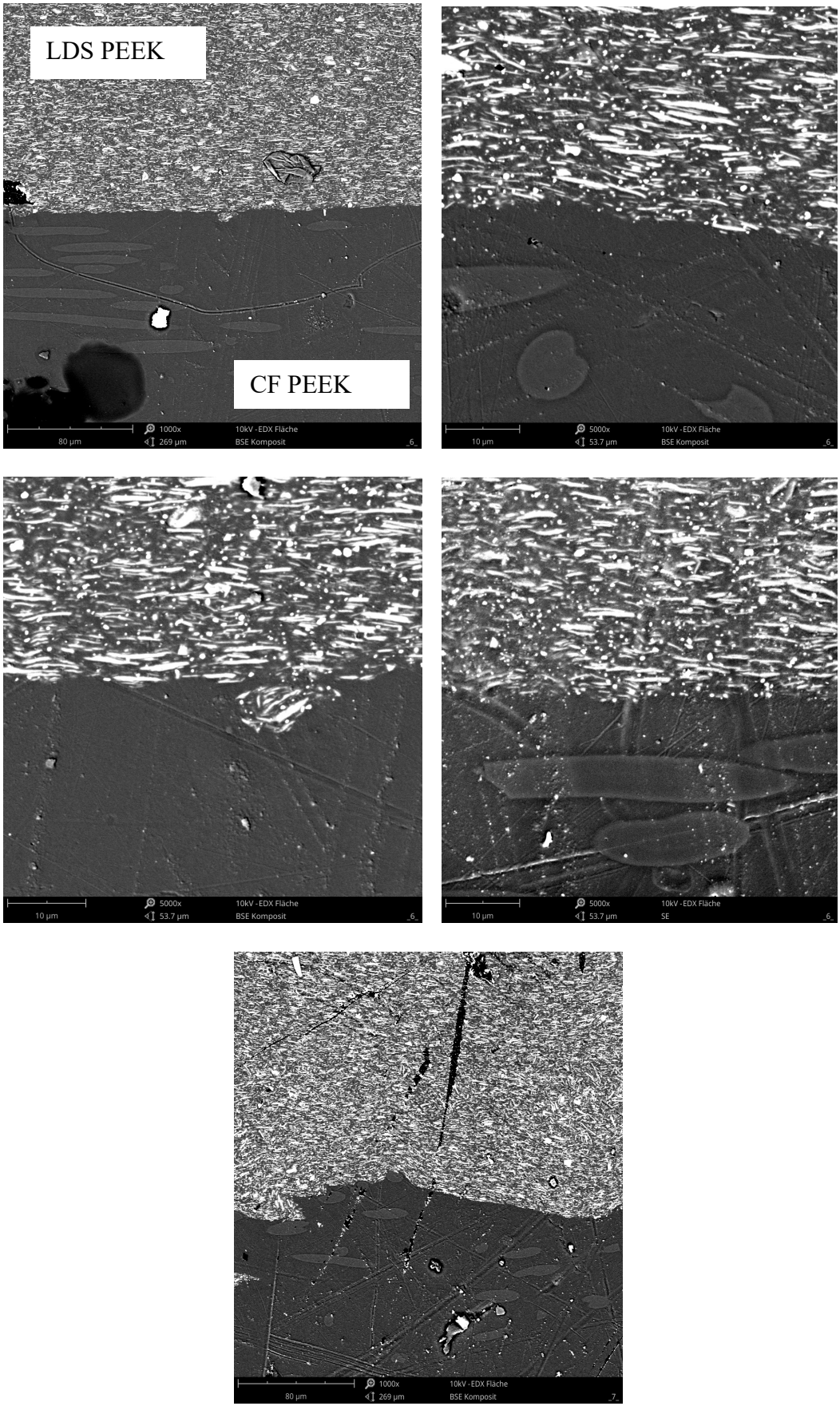

Figure 4-19: Phenom XL SEM images of interlayer bonding

The SEM analysis further corroborates the observations from optical microscopy, providing higher-resolution evidence of a well-fused interface between the CF-PEEK and LDS-PEEK layers. The images reveal a continuous and defect-free transition zone, with no detectable voids, cracks, or delamination along the interlayer boundary. The LDS-PEEK is seen to be uniformly deposited on the CF-PEEK substrate, ensuring intimate contact and strong adhesion across the interface. Moreover, the microstructural continuity confirms that the thermal bonding achieved during the FFF process was sufficient to prevent interfacial separation, thereby validating the structural integrity of the hybrid material system.

5 Conclusions

The objective of this work was to investigate the dimensional accuracy, warpage behavior, and interlayer bonding of CF-PEEK and LDS-PEEK parts fabricated by FFF, with particular emphasis on the challenges of dual-material printing. While extensive literature exists on PEEK and CF-PEEK processing, studies on LDS-PEEK are absent, leaving its printability and interaction with CF-PEEK unexplored.

1. We demonstrated that post-print heat treatment, specifically synchronous cooling of both chamber and bed in stepped ramps, was essential to minimizing residual stress. This strategy reduced top–bottom temperature gradients and greatly improved flatness.
2. We measured the dimensional flatness of CF-PEEK panels under different infill orientations and cooling strategies, showing that infill pattern is a dominant factor influencing warp. Aligned rectilinear infill at 0° was identified as the most stable baseline, reducing variance and enabling consistent comparison across tests.
3. We showed that thermal conditions (bed, chamber, and layer heater) strongly impact dimensional accuracy. Results from ANOVA and response surface modelling demonstrated that moderate chamber (~255 °C) and bed (~260 °C) settings minimize flatness deviation, while extremes in either direction increase warpage.
4. The obtained results showcase that dimensional accuracy in the Z-direction is governed primarily by the layer heater temperature, which improves parts consolidation but drives systematic thinning at elevated values when parts are thin. The bed temperature further stabilizes flatness at 200–270 °C but reinforces thinning effects when raised above 280 °C.
5. We found that LDS-PEEK, when printed alone, exhibited excellent surface quality and dimensional stability across all infill orientations, with no need for post-processing or annealing.
6. We showed that in dual-material printing, warping became significant when LDS-PEEK was deposited on CF-PEEK with matching raster orientations. This effect is mainly explained by the mismatch in coefficients of thermal expansion (CTE) between the reinforced and unfilled PEEK grades.
7. We found through Design of Experiments that raster angle is the most dominant factor affecting flatness deviation in dual-material prints, followed by layer height. A low raster

angle (0°) and minimal layer height (0.125 mm) yielded the best results, while the number of LDS layers had only a minor influence.
8. We showed that the optimized parameter set; layer height 0.125 mm, two LDS layers, and 0° raster angle in rectilinear infill, resulted in a very low predicted thickness error (0.11%) and flatness deviation (0.70 mm), with a desirability value of 0.998, confirming the robustness of this solution.
9. We found through microscopic examination that the CF-PEEK and LDS-PEEK interface formed a continuous bond, with carbon fibers occasionally penetrating the LDS-PEEK region, suggesting localized mechanical interlocking and absence of major voids or delamination.

This work establishes a comprehensive framework for optimizing the FFF printing of CF-PEEK and dual-material CF-PEEK/LDS-PEEK systems. It demonstrates how infill orientation, thermal environment, and layer parameters interact to determine dimensional stability, and identifies a near-optimal parameter window for dual-material printing. Furthermore, it provides first experimental evidence of successful interlayer bonding between CF-PEEK and LDS-PEEK, offering a pathway for multifunctional CubeSat panel fabrication.

Suggestions for further work

Future studies could:

- Extend dimensional accuracy studies to larger geometries beyond 70 × 70 mm to assess scalability.
- Investigate microstructural and crystalline changes in the LDS-PEEK layer under varying cooling.
- Investigate how the different printing parameters of LDS PEEK affect the laser direct structuring processing.
- Explore long-term thermal cycling and mechanical testing of CF-PEEK/LDS-PEEK interfaces to validate structural integrity under aerospace conditions.

Bibliography

[1] N. S. Gorella, M. Caruso, P. Gallina and S. Seriani, "Dynamically balanced pointing system for CubeSats: Study and 3D printing manufacturing," *Robotics,* vol. 10, no. 4, p. 569–571, 2021.

[2] A. Caparrós and J. Becedas, "Additive manufacturing applied to the design of small satellite structure for space debris reduction," in *Applications of Design for Manufacturing and Assembly*, vol. 10, Intechopen, 2018.

[3] A. Boschetto, L. Bottini, L. Macera and S. Vatanparast, "Additive manufacturing for lightweighting satellite platform," *Applied Sciences,* vol. 13, no. 2809, February 2023.

[4] P. Wang, B. Zou, S. Ding, L. Li and C. Huang, "Effects of FDM-3D printing parameters on mechanical properties and microstructure of CF/ PEEK and GF/PEEK," *Chinese Journal of Aeronautics,* vol. 34, no. 9, 2021.

[5] "Orion Additive Manufacturing," [Online]. Available: https://www.orion-am.com/3d-printing-service.

[6] A. Jadhav and V. S. Jadhav, "A review on 3D printing: An additive manufacturing technology," *Materials Today: Proceedings,* vol. 62, 2022.

[7] J. R. C. Dizon, A. H. E. Jr., Q. Chena and R. C. Advincul, "Mechanical characterization of 3D-printed polymers," *Additive Manufacturing,* vol. 20, 2018.

[8] C. Schmutzler, A. Zimmermann and M. F. Zaeh, "Compensating Warpage of 3D Printed Parts Using Free-form Deformation," *Procedia CIRP,* vol. 41, 2016.

[9] J. Herzberger, J. M. Sirrine, C. B. Williams and T. E. Long, "Polymer Design for 3D Printing Elastomers: Recent Advances in Structure, Properties, and Printing," *Progress in Polymer Science,* vol. 97, no. 101144, 2019.

[10] J. Abel, U. Scheithauer, H. Klemm and T. Moritz, "Additive manufacturing of ceramic parts through fused-filament-fabrication," Fraunhofer IKTS, 2017.

[11] S. H. Adarsh and N. Mahadevappa, "Effect of Printing Parameters on Mechanical Properties and Warpage of 3D-Printed PEEK/CF-PEEK Composites Using Multi-

Objective Optimization Technique," *Journal of Composites Science,* vol. 9, no. 8, 2025.

[12] N. Harsha P. S, P. Nagaraju, S. Y. Sonaye, V. K. Bokam and P. Sikder, "In-house processing of carbon fiber-reinforced polyetheretherketone (CFR-PEEK) 3D printable filaments and fused filament fabrication-3D printing of CFR-PEEK parts," *The international journal of advanced manufacturing technology ,* vol. 128, 2023.

[13] A. Álvarez-Trejo, E. Cuan-Urquizo, D. Bhate and Armando Roman-Flores, "Mechanical metamaterials with topologies based on curved elements: An overview of design, additive manufacturing and mechanical properties," *Materials & Design,* vol. 223, no. 112190, 2023.

[14] J. P. Dinis Lopes, "Effect of the ironing process on parts produced by Fused Filament Fbarication," Tecnico Lisboa, 2021.

[15] C. C. Santiago, B. Yelamanchi, J. A. D. D. l. Peña, J. Lamb, K. Roguski, F. Turzyński, R. Faruqui, K. Choo, A. D. Plessis, F. Silani, E. MacDonald and P. Cortes, "Thermoplastic Extrusion Additive Manufacturing of High-Performance Carbon Fiber PEEK Lattices," *Crystals,* vol. 11, no. 1453, 2021.

[16] H. Zhou, X. C. 1, X. Jiang, G. Zheng, J. Zhang, Y. Li, M. Tang and F. Lv, "Green Manufacturing-Oriented Polyetheretherketone Additive Manufacturing and Dry Milling Post-Processing Process Research," *Processes ,* vol. 10, no. 2561, 2022.

[17] D. Yavas and L. Sosa, "Investigating the interlaminar shear strength of short carbon fiber-reinforced PEEK composites fabricated by fused filament fabrication," in *International Mechanical Engineering Congress and Exposition IMECE*, New Orleans, 2023.

[18] A. Bogdanov, Eremin, Alexander, M. Burkov, S. Panin and P. Lyubutin, "Estimating degradation of strength of neat PEEK and PEEK-CF laminates under cyclic loading by mechanical hysteresis loops," *Fracture and structural integrity,* vol. 17, no. 66, 2023.

[19] Z. Wang, B. Zhang and L. Yuxuan, "Mechanical characterization of PEEK-CF/PEEK sandwich structures prepared via a combination of fused filament fabrication and epoxy post-bonding," *Journal of adhesion science and technology ,* vol. 38, no. 17, 2023.

[20] "cylex," [Online]. Available: https://cylexplastics.com/carbon-fiber-reinforced-peek-performance-advantages-and-technological-innovations-of-peek-cf30/..

[21] A. Friedrich, M. Fengler, B. Geck and D. Manteuffel, "60 GHz 3D Integrated Waveguide Fed Antennas Using Laser Direct Structuring Technology," in *European Conference on Antennas and Propagation (EUCAP)*, Paris , 2017.

[22] J. Ramian, J. Ramian and D. Dziob, "Thermal Deformations of Thermoplast during 3D Printing: Warping in the Case of ABS," *Materials,* vol. 22, no. 7070, 2021.

[23] S. L. uo Liang Goh, S. H. Cheng, D. J. S. Goh, P. Laya, V. P. Nguyen, B. S. Han and W. Y. Yeong, " Enhancing interlaminar adhesion in multi-material 3D printing: A study of conductive PLA and TPU interfaces through fused filament fabrication," *Materials Science in Additive Manufacturing,* vol. 3, no. 2672, 2024.

[24] T.-M. Wang and J.-T. J. X. Xi, "A model research for prototype warp deformation in the FDM process," *International Journal of Advanced Manufacturing Technology,* vol. 33, 2007.

[25] L. Benedett, B. Brulé, N. Decreamer, K. Evans and O. Ghita, "Shrinkage behaviour of semi-crystalline polymers in laser sintering: PEKK and PA12," *Materials & Design,* no. 181, 2019.

[26] D. Yang, Y. Cao, Z. Zhang, Y. Yin and D. Li, "Effects of crystallinity control on mechanical properties of 3D-printed short-carbon-fiber-reinforced polyether ether ketone composites," *Polymer Testing ,* vol. 97, no. 107149, 2021.

[27] V. S. Vakharia, H. Leonard, M. Singh and M. C. Halbig, "Multi-Material Additive Manufacturing of High Temperature Polyetherimide (PEI)–Based Polymer Systems for Lightweight Aerospace Applications," *Polymers,* vol. 15, no. 561, 2023.

[28] J. Ahmad and M. G. Niasar, "Aging Behavior of PEEK, PTFE, and PI Insulation Materials Under Thermal Oxidative and Humid Conditions for Aerospace Applications," *Journal of Applied Polymer Science,* vol. 142, no. 19, 2025.

[29] A. Dean, D. Voss and D. Danel, Design and Analysis of Experiments, Springer, 2017.

[30] Q. F. David Humbird, "Scale-Up Considerations for Biofuels," in *Biotechnology for Biofuel Production and Optimization*, Elsevier, 2016.

[31] J. Wang and W. Wan, "Experimental design methods for fermentative hydrogen production: A review," *International Journal of Hydrogen Energy,* vol. 34, no. 1, 2009.

[32] N. Szpisják-Gulyás, A. N. Al-Tayawi, Z. Horváth and Z. László, "Methods for experimental design, centralcomposite design and the Box–Behnken design, tooptimise operational parameters: A review," *Acta Alimentaria,* vol. 52, 2023.

[33] SOLVAY, "Technical Data Sheet KetaSpire CF10 LS1 AM Filament," 2022.

[34] Ensigner, "TECAFIL PEEK LDS black - 1.75 mm - Filament," 2024. [Online]. Available: https://www.ensinger-online.com/modules/public/sheet/createsheet.php?SID=3233&FL=0&FILENAME=TECAFIL_PEEK_LDS_black_0.PDF&ZOOM=1.0.

[35] A. R. Zanjanijam, I. Major, J. G. Lyons, U. Lafont and D. M. Devine, "Fused Filament Fabrication of PEEK: A Review of Process-Structure-Property Relationships," *Polymers,* vol. 12, no. 8, 2020.

[36] S.-L. Gao and J.-K. Kim, "Cooling rate influences in carbon fibre/PEEK composites. Part 1. Crystallinity and interface adhesion," *Composites Part A: Applied Science and Manufacturing,* vol. 31, no. 6, 2000.

[37] W. Wu, P. Geng, G. Li, D. Zhao, H. Zhang and J. Zhao, "Influence of Layer Thickness and Raster Angle on the Mechanical Properties of 3D-Printed PEEK and a Comparative Mechanical Study between PEEK and ABS," *Materials,* vol. 8, no. 9, 2015.

[38] A. Boschetto and L. Bottini, "Accuracy prediction in fused deposition modeling,," *International Journal Advanced Manufacturing Technology ,* vol. 73, 2014.

[39] B. N. Turner, R. J. Strong and S. A. Gold, "A review of melt extrusion additive manufacturing processes: I. Process design and modeling," *Rapid prototyping Journal ,* vol. 20, no. 3, 20114.

[40] G. Dai, L. Zhan, C. Guan and M. Huang, "The effect of cooling rate on crystallization behavior and tensile properties of CF/PEEK composites," *Journal of Polymer Engineering,* vol. 41, no. 6.

[41] S. Prabhu, M. Uma, J. Jaishwin and M. Nikhil, "Experimental Study and Predictive Modelling of Fused Deposition Modelling (FDM)," *International Journal of Automotive and Mechanical Engineering (IJAME),* vol. 20, no. 1, 2023.

[42] G. S. Robles, R. N. M. Delda, R. L. B. d. Rosario, M. T. Espino and J. R. C. Dizon, "Dimensional Accuracy of 3D - Printed Acrylonitrile Butadiene Styrene: Effect of Size, Layer Thickness, and Infill Density," *Key Engineering Materials ,* vol. 913, 2022.

[43] A. Greco, A. De Luca, R. Sepe and S. Gerbino, "Investigation on tensile properties of FFF PEEK: Effects of printing parameters and post-processing treatment," *rocedia Structural Integrity,* vol. 53, 2024.

[44] Q. Sun, ZhongdeShan, L. Zhan, S. Wang, X. Liu, Z. Li and S. Wu, " Warp deformation model of polyetheretherketone composites reinforced with carbon fiber for additive manufacturing," *Material Research Express,* vol. 8, 2021.

[45] A. K. Sood, R. Ohdar and S. Mahapatra, "Improving dimensional accuracy of Fused Deposition Modelling processed part using grey Taguchi method," *Materials and Design ,* vol. 30, 2009 .

[46] "StatEase,"[Online].Available: https://www.statease.com/docs/se360/contents/analysis/confirmation/#confirmation.